UNIVERSITÀ DEGLI STUDI DI PADOVA

UNIVERSITA' DEGLI STUDI DI PADOVA

Dipartimento di Ingegneria Industriale DII

Corso di Laurea Magistrale in Ingegneria dell'Energia Elettrica

Modelling, Simulation and Analysis of a Buck-Boost Converter for Photovoltaic Application

Modello, Simulazione ed Analisi di un Convertitore Buck-Boost per Applicazione Fotovoltaica

Relatore: Prof. Roberto Turri

Correlatori: Prof.ssa Marta Molinas
Ing. Noe Barrera Gallegos

Francesco Andreis 1132403

Anno Accademico 2017/2018

Abstract

Power production from photovoltaic panels is strongly dependent on meteorological conditions. This means that when weather changes occur, for example cloud transients, fluctuations in the irradiance produce changes in the power production. PV systems connected to the traditional AC grid induce those power fluctuations into the AC grid. This may have some effect in the stability of the AC grid, both on its frequency and voltage amplitude, and on the stability of the DC side, in case the power source wasn t directly connected to the utility grid by means of an AC to DC converter.

One of the typical structures when connecting a photovoltaic power source to the AC grid is formed by a buck-boost converter, a BESS (Battery Energy Storage System) controlled by a DC-DC converter like a boost; this will allow to store energy when power production is higher than the instantaneous demand, that will eventually be used when the power request exceeds its production. This system also permit to control the voltage, stabilising it to a constant value in the DC link in spite of the fluctuations of the power produced, due to changes in weather conditions.

The power produced by a photovoltaic source is dependent on solar irradiation and temperature. Starting from the values obtained from a real data sheet, the parameters of the one diode model are extracted, in order to be able to simulate current and voltage produced by the panel under every meteorological condition. A Maximum Power Point Tracking algorithm needs to be implemented to extract the maximum available power from the photovoltaic system, this algorithm will perform controlling the duty-cycle of the buck-boost converter in order to operate the panel under the desired output voltage. The battery is also modelled and fit in the simulation. A control is developed to regulate the charge and discharge operations and to protect the battery from possible faults.

Finally the inverter connecting the DC side to the AC grid is modelled, together with its control. Using this model we are able to simulate with enough detail and eventually perfom a stability analysis.

This simulations will allow to study both its linear and non-linear behaviour when sudden variations in meteorological conditions will influence current, voltage and power produced by the panel, changing therefore the point of operation of the system. The average model of the converter will be confronted and verified with its respective switched model. This will permit to introduce some reasonable simplifications and focus on the transient response of the system.

Sommario

In questo lavoro, svolto all NTNU di Trondheim, Norvegia si sviluppa un modello di una microrete in corrente continua, nella quale sono presenti una fonte di generazione fotovoltaica connessa ad un convertitore buck-boost, in parallelo si connette alla rete DC tramite un ulteriore convertitore buck-boost una batteria a piombo-acido, infine un convertitore DC/AC connette la suddetta rete ad una rete in alternata con frequenza di 60 Hz. Per fare ciò si è utilizzato il software di simulazione Simulink.

Questo progetto è parte di un lavoro di ricerca più ampio, condotto dall Ignegnere Noe Barrera Gallegos, sotto la supervisione della Professoressa Marta Molinas.

Lo scopo della tesi è di verificare l affidabilità del modello del convertitore buck-boost, il quale viene costruito sulla base valori medi che questo manifesta in condizioni di regime (averaged model). Il controllore proporzionale-integrativo adibito al controllo della tensione d ingresso per il convertitore connesso al pannello fotovoltaico, e d uscita per quello connesso alla batteria, viene derivato sulla base di una forte, ma efficace semplificazione. Con i valori scelti per i componenti del sistema si ottiene una funzione di trasferimento con due poli reali negativi, ciò significa che il sistema è stabile se controllato opportunamente. Tra i due poli inoltre, ve n è uno molto più grande in modulo dell altro, ciò significa che esso determina il comportamento del sistema nei primi istanti, con un regime transitorio che si estingue molto prima di quello legato all altro polo. Poichè si sta studiando un modello basato sui valori medi nel tempo delle varie grandezze, si può trascurare il polo più grande in valore assoluto dei due poli, ottenendo una funzione di trasferimento semplificata.

Tramite un analisi parametrica effettuata sui due componenti del convertitore che fungono da serbatoio di energia, ovvero che garantiscono la conduzione quando l input del buck-boost rappresentato dal pannello fotovoltaico o dalla batteria è scollegato dall output perchè l interruttore è aperto, si è verificato come sia l induttanza a giocare il ruolo principale nel controllo delle grandezze tensione e corrente. Il condensatore presente nell output influenza il ripple della tensione, ovvero il comportamento alle frequenze più alte, in quanto legato all altro polo della funzione di trasferimento. Esso sarà quindi fondamentale per stabilizzare la tensione, riducendone il contenuto armonico.

Il convertitore del pannello fotovoltaico è adibito al controllo di questo, in modo da farlo operare nel punto di massima potenza al variare delle condizioni meteorologiche ed ambientali. Ciò viene conseguito tramite un algoritmo di controllo, il quale opera regolando la tensione di uscita del pannello fotovoltaico portandolo a lavorare in un dato punto della caratteristica tensione-corrente ottenuta in precise condizioni ambientali, per il quale il pannello produce la massima potenza possibile. Questo sistema viene anche chiamato Maximum Power Point Tracking System (MPPT System).

L algoritmo scelto per tracciare le migliori condizioni di lavoro viene definito di conduttanza incrementale. Esso campiona tensione e corrente prodotte dal pannello e le confronta con i valori campionati nell istante precedente, inoltre confronta il rapporto della differenza tra i campionamenti di corrente e tensione con il rapporto di corrente e tensione dell ultimo campionamento, aumentando o diminuendo il valore di riferimento della tensione di conseguenza.

La batteria di conseguenza, è necessaria per mantenere costante la tensione della rete in DC, in modo di garantire una conversione DC/AC più stabile. Infatti per dare libertà di funzionamento al pannello fotovoltaico, il quale produce sempre la massima potenza che gli viene consentita, la batteria dovrà immagazzinare o cedere energia dipendentemente dal fatto che la domanda superi la produzione, o viceversa. Questo si può conseguire tramite il convertitore

associato a questa, che mantiene costante la sua tensione di uscita indipendentemente da ciò che accade, fintanto che vi è abbastanza energia immagazzinata nella batteria.

Anche questa è stata implementata nella simulazione tramite un modello basato su un circuito elettrico equivalente. Poichè è una tecnologia ancora in fase di svilupo e vi sono molti modelli diversi in letteratura che cercano, con differenti livelli di complessità e accuratezza, di riprodurre il suo comportamento, e data la complessità di questi, si è deciso di utilizzare il modello fornito da Simulink.

Infine la conversione da continua ad alternata viene compiuta da un convertitore monofase a tensione impressa, il quale connette il lato in continua alla rete in alternata. Esso opera in un sistema di riferimento sincrono, rotante alla stessa frequenza delle grandezze di rete, in modo da ottenere grandezze costanti nel tempo e consentire l utilizzo di controllori proporzionali-integrativi, ottendo così errori nulli a regime; inoltre il controllo della potenza attiva e reattiva è semplificato in quanto queste sono indipendenti, dipendendo da grandezze diverse. Per ottenere questa condizione si fa utilizzo di un PLL (Phase-Locked Loop), il quale tramite misurazioni sulla tensione, regola la velocità di rotazione del sistema di riferimento e la sua fase, in modo tale da rintracciare la frequenza di rete.

Uno studio dettagliato del convertitore è stato eseguito all interno del progetto di ricerca condotto dall Ing. B. Gallegos, dallo studente Sigurd Strømsem, il quale ha studiato il comportamento del convertitore, costruendo un modello lineare, e del PLL. Il suo lavoro è stato presentato nella tesi magistrale da lui realizzata, la quale analizza sia il comportamento lineare del PLL, sia quello non lineare, verificando se il modello costruito è in grado di rintracciare propriamente la frequenza di rete, anche in condizioni non ideali. I risultati da lui ottenuti sono stati utilizzati in questo lavoro al fine di completezza, fornendo un modello ed un analisi completi.

L ultima parte di questa tesi infatti analizza e verifica se le non linearità introdotte dai vari componenti (il pannello fotovoltaico, l algoritmo di rintracciamento del punto di massima potenza, la batteria e il PLL) influiscono sul modello del convertitore buck-boost sviluppato e sul suo sistema di controllo. Operando infatti con modelli basati sui valori medi, si presuppone infatti di essere in condizioni operative che non si discostano eccessivamente dai valori di regime. I sistemi di controllo sviluppati devono quindi essere validati, tramite confronto con modelli reali, detti switched models, i quali tengono conto degli interruttori e delle frequenze da essi indotte nell impianto.

Nel costruire la simulazione generale infatti, si sono prima analizzati i singoli componenti, i quali sono poi stati inglobati nel modello, verificando di volta in volta gli effetti che essi inducono alla stabilità della simulazione.

Questo lavoro vuole essere un aiuto per comprendere meglio le conseguenze che fenomeni non lineari hanno su un modello basato su dei valori medi nel tempo, che sfrutta quindi la linearità del sistema.

Preface

This thesis is submitted to the University of Padova (Università degli Studi di Padova) for fulfilment of the requirements for the master degree in Electrical Energy Engineering (Ingegneria dell Energia Elettrica).

The work was carried out at the Department of Engineering Cybernetics at the Norwegian University of Science and Technology (NTNU) through the Erasmus+ program, under the supervision of Prof. Marta Molinas and Ing. Noe Barrera Gallegos. It is part of a wider research project and, where reported, work performed by other people who were part of it is used.

Acknowledgments

I would first like to thank Ing. Noe Barrera Gallegos who followed and supervised me in this task. He was always helpful and available for all my needs.

I would also like to thank Prof. Marta Molinas for accepting me as an exchange student and allowing me to work under her supervision at the Department of Engineering Cybernetics of NTNU, in Trondheim.

Last but not least, I must thank my family for supporting me throughout my years of study.

Contents

List of Figures

List of Tables

Chapter 1

Introduction

This chapter will present the motivations that induced this work, giving a general view on the state of art of photovoltaic energy production. The outline of the thesis is then presented.

1.1 Motivation

Due to the concerns about climate changes and the finite availability of fossil fuels, renewable energy sources have been gaining popularity in the last decades. In the last years they have become available at convenient prices thanks to technology improvements, development of new materials and subsidies provided by a lot of governments, and an increase in power produced from renewable energy sources has been noticed. Figure 1.1 [1] shows how solar power is becoming a relevant energy source. The two main renewable sources at the moment are solar and wind energy. They are clearly not always available during the day: the peak of photovoltaic production is around mid day; while despite the accurate choice for the installation of a wind power plant, wind is not always present and it s not even constant in most of the locations. All these factors lead to a series of problems regarding the control of these sources and their connection to the grid, which must be studied and solved.

An example of a possible issue is here reported. On the 18th of May 2011 in Sicily, an Italian region, a steam powered power plant was disconnected from the 220 kV grid due to a failure, while delivering approximately 150 MW. This brought the frequency to drop below a value of 49.7 Hz and led to the disconnection of all DER (Distributed Energy Resources) in the Region, composed mainly of photovoltaic plants, for an additional loss of about 210 MW [2]. This induced a further frequency drop in the grid to a value of 49 Hz until it was restored within the legal standards. This fault lasted 8 seconds and caused the disconnection of some loads from the grid as safety measure. Faults like this happen because a protection system acts disconnecting the photovoltaic source when certain conditions are reached, that could be dangerous for system stability or for the components of the microgrid itself.

Microgrids appear to be a good solution to cope with these problems. They are a new concept in the way of realizing energy distribution: they combine efficiently Distributed Generation (DG) systems with energy storage systems thanks to some advanced control methods. Furthermore they can also operate both connected to the AC grid or islanded from it. As the name suggest, microgrids are small AC or DC grids that settle and control power generation in an area close to its consumers or, how they ve been called recently, prosumers, since they both produce and consume energy. Because of these reasons, microgrids can give more flexibility to the overall grid, but efficient control methods must be developed to coordinate all parts of the system and to produce and deliver power following specific requirements on stability and power quality.

1.2 Goal of the Thesis

The behaviour of such systems is complex because a lot of variables have to be considered, and it s non-linear. Approximations can be made, representing the model with a linear behaviour,

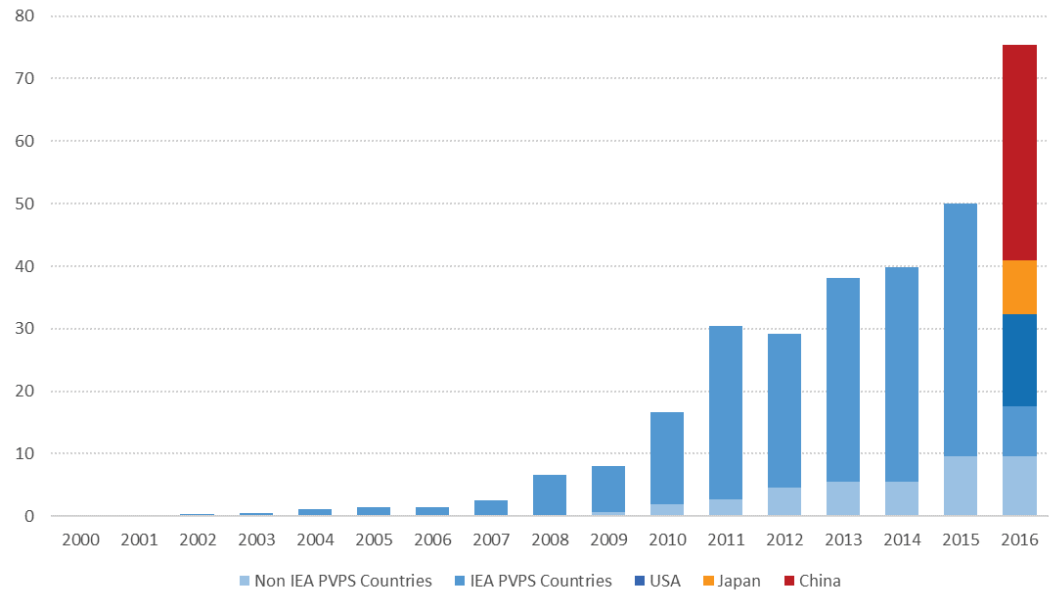

Figure 1.1: Evolution of annual photovoltaic power installation [GW].

but it must be proved that such approximations do not affect its accuracy. One of the main challenges is to develop a control system that allows to produce power with the maximum efficiency, integrates an energy storage system and is able to work correctly under different operating conditions, assuring stability. The main goal of the thesis is therefore to model a system composed by a photovoltaic source, its converter and a maximum power point tracking system, a battery with its relative converter, and a converter to transmit power from DC to AC, that will be simulated to understand which parameters influence mainly its response, and how much a linear model differs from the more realistic switched one. The effects of working in a point different from the steady state operation must be analysed to verify that the control is suitable for different situations.

These system have a significant non linear behaviour, that must be studied. Average models are in fact often used to simulate converters, and they provide a good approximation of their response, but it must be verified whether these models can provide also an accurate dynamic together with non linear components such as a battery or a photovoltaic panel. The conversion from DC to AC is ensured by a converter, with a phase-locked loop that tracks the grid frequency; this is a further element of instability that must be studied.

The PV panel needs to produce the maximum power, this is achieved implementing an algorithm on the control of its relative inverter that will track the maximum power point in spite of cloud transients and changes in environmental conditions. The battery will help holding the voltage to a stable value on the DC line, charging and discharging operations will be controlled by a converter connecting it to the DC grid.

Different models have been presented in literature, and simplifications have been made to try to clarify the response of such a system. The aim of this work is to improve the understanding of this behaviour, working with a level of detail more advanced than the basic average model, which focuses on steady state operations. This is in fact used to model the converters but the complete behaviour is studied, analysing specifically the non-linear response to step changes in the inputs, and the consequences that these induce in power production, in the voltage control and in the phase tracking system of the DC/AC converter.

The degree of detail is therefore more advanced than the standard average model, but less complicated than the switched model, enabling the possibility to simulate rapidly and for a longer time span, studying both the reaction of the system during the transitory and during steady state operations.

1.3 Thesis outline

The first chapter introduces the motivation for this work giving a brief overview on the main problems. The goal of the thesis is then exposed, followed by an outline of this.

The second chapter deals with the modelling of the photovoltaic panel, describing the photovoltaic effect and the physics involved in the generation of electrical current first, then the dependence on external parameters is introduced. Afterwards the single-diode model is exposed and its various parameters are calculated, the dependence on temperature and irradiance is verified and the model is fit in a simulation with Simulink. Different maximum power point tracking method are shown and one is chosen and developed to be included in the model, operating on the DC/DC converter that connects the PV panel to the DC bus.

In the third chapter the converter connecting the photovoltaic panel to the DC grid is modelled. A first model controlling the output voltage was developed, with the objective of understanding the influence of the components involved. The values of the elements of the converter are then calculated, starting from specific constraints on voltage and current ripple. Once the role of the different components is clear, the model and control of the input voltage, that is the output of the photovoltaic panel, are developed. The average model is then simulated together with the switched model of the same converter, confronting them and verifying its reliability.

Chapter 4 briefly introduces the energy storage system, modelling the battery.

Chapter 5 presents the DC/AC converter and its phase-locked loop. This task was fulfilled in parallel by the student Sigurd Strømsem in his master s thesis, that focused specifically on the study of this converter. Here the theoretical background and the necessary parts for this work are explained, and the converter is fitted in this model.

Chapter 2

Photovoltaic Panel

This chapter will deal with the photovoltaic energy source, briefly explaining the physical principles behind it, modelling the panel, calculating the involved parameters and implementing the maximum power tracking system.

2.1 Photovoltaic Cell

The photovoltaic effect was discovered in 1839 by the Becquerel family [3]. It consists in the conversion of solar irradiance into electricity. A photovoltaic cell consists of a wafer formed mainly by two semiconductor materials, generally silicon (Si) doped differently, and connected together forming a p-n junction. When the cell is subjected to solar irradiance, the PV effect happens only if the energy of incident photons is greater than the band gap of the semiconductor, 1,12 eV for silicon [4].

When solar radiation is absorbed in the material, it transfers part of its energy to the atoms in its structure and, if it is the right quantity it will excite an electron and move it to the conduction band An electron-hole pair is therefore generated. The electric field in the junction will then separate them and if the cell is connected to an external load by means of some electrodes, a DC current is established.

This phenomenon is strictly dependent on the materials involved and on the wavelength of incident light [5]: different materials have different band gaps and the energy of the incoming wave must not be too small or too big. Voltage and current produced by a singular cell are too small, different cells are connected then in series to raise the output voltage and in parallel to increase the delivered current. For a given irradiance and temperature the typical characteristic of a (silicon) photovoltaic panel is given in figure 2.1.

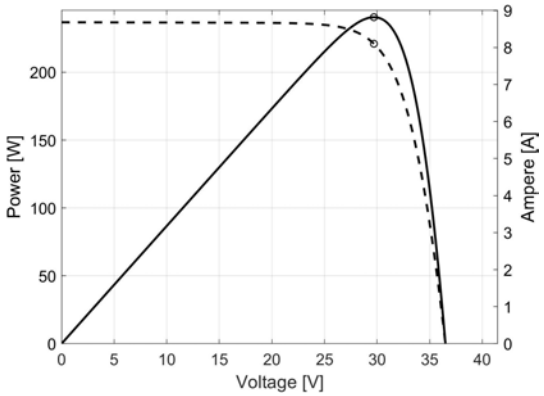

Figure 2.1: Example of a characteristic of a solar cell with given irradiance and temperature. The dotted line represents current profile for different voltage values, the continuous line shows power vs voltage profile. The point where the maximum power is produced is highlighted.

It can be seen how the module behaves as a current source from low voltages up to a certain point where, after a transition phase, its behaviour changes into a voltage source. The characteristic changes if environmental conditions change as well. It mainly depends on irradiance and temperature. It can be noticed from figure 2.2a that the produced current depends strongly on the irradiance level, this is because with a stronger irradiance more energy is transferred to the atoms, therefore more electrons move from the valence band to the conduction band [6].

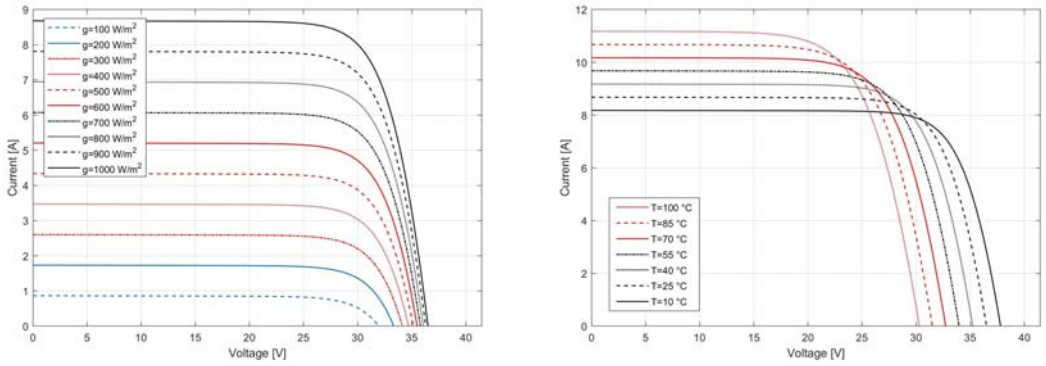

(a) Temperature= 25 °C, varying irradiance. (b) Irradiance = 1000 W/m^2, varying temperature.

Figure 2.2: Current-Voltage characteristics of a solar cell varying external conditions.

On the other hand, voltage depends principally on temperature. This comes from the fact that the open circuit voltage V_{oc}, that is the maximum voltage obtained from a solar cell with null produced current, is determined by the value of the reverse saturation current I_0 [7]. This is a measure of the leakage of minority carriers across the p-n junction in reverse bias, as a result of carrier recombination in the neutral region of either side of the junction. Since the minority carriers are thermally generated, this results in a dependence of V_{oc} on temperature, and consequently the characteristic is shifted left for increasing temperature as shown in figure 2.2b[1].

Figure 2.3 shows as both this effects give a reduction of produced power, which is more evident in 2.3a because of the stronger effect of irradiance on current than the one of temperature on voltage. As a result it s clear that the cell should work at different specific voltage values in order to extract the maximum power in all various environmental situations. It is also noticeable that, taken a particular characteristic corresponding to some specific conditions, if the photovoltaic cell is not operated with the optimal voltage the maximum power can not be extracted. In fact the power generated can vary considerably if the operation point is slightly shifted left or right along the curve. Thus a maximum power tracking system is required to run the photovoltaic system at its maximum possible efficiency.

2.2 Panel Modelling

In order to simulate the PV panel a model must be developed. A lot of different models can be found in literature, with various level of complexity and accuracy. The single-diode model has been chosen for its higher simplicity than the double-diode one, nevertheless precision of the results is not substantially affected. The model is composed by a current source representing the generation of current I_{ph} from the photovoltaic effect, its intensity is hence proportional to irradiation. A diode in parallel to it symbolizes the non-linear phenomena like diffusion and recombination, by means of a current I_D flowing through it. Finally two resistors, one in parallel R_{sh} and one in series R_s, refine the model representing respectively leakage current in the p-n junction and structural resistances in the module.

Figure 2.4 [8] portrays the model, that will now be described in detail. The circuit is

[1] All figures were obtained simulating a photovoltaic model with Matlab.

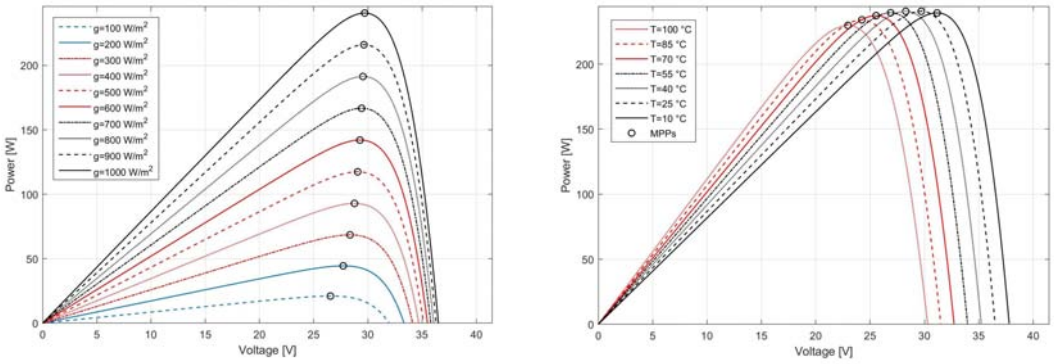

(a) Temperature= 25 °C, varying irradiance. (b) Irradiance= 1000 W/m^2, varying temperature.

Figure 2.3: Power-Voltage characteristics of a solar cell varying external conditions.

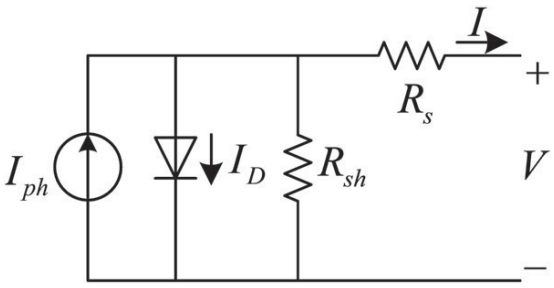

Figure 2.4: Single-diode equivalent circuit representation.

characterized by the equation:

$$\begin{aligned} I &= I_{ph} - I_D - I_{R_{sh}} \\ &= I_{ph} - I_0 \left(\exp\left(\frac{V + R_s I}{N_s n V_t} \right) - 1 \right) - \frac{V + R_s I}{R_{sh}} \end{aligned} \tag{2.1}$$

where V and I are output current and voltage of the photovoltaic panel, I_0 is the diode reverse saturation current, N_s is the number of series connected cells in the photovoltaic panel, n is the diode ideality factor and V_t is the thermal voltage, that is defined as:

$$\begin{aligned} V_t = \frac{k_B T}{q} \qquad & k_B = \text{Boltzmann constant} \\ & T = \text{Panel temperature in Kelvin} \\ & q = \text{Electron charge} \end{aligned} \tag{2.2}$$

To implement the model into a simulation, all this parameters must be calculated first. They are not given on the specifications by the panel manufacturers. In this case too, a lot of different ways to compute the involved quantities can be found in literature. It has been chosen here to calculate them with a numerical method, solving four non-linear equation. Three points found on the data sheets, i.e. open circuit $(V_{oc}, 0)$, short circuit $(0, I_{sc})$ and MPP (Maximum Power Point) (V_{mpp}, I_{mpp}), are fitted into equation 2.1. This values are given for standard conditions (STC), that is with irradiance equal to 1 kW/m^2 and temperature of 25 °C [8, 9, 10]. A fourth equation then is obtained from the fact that at the short circuit point on the V-I characteristic the slope of the curve is equal to $-1/R_{sh}$.

Naming $\gamma = N_s n$, from the first three conditions we get:

$$0 = I_{ph} - I_0 \left(\exp\left(\frac{V_{oc}}{\gamma V_t} \right) - 1 \right) - \frac{V_{oc}}{R_{sh}} \tag{2.3}$$

$$I_{sc} = I_{ph} - I_0 \left(\exp\left(\frac{R_s I_{sc}}{\gamma V_t} \right) - 1 \right) - \frac{R_s I_{sc}}{R_{sh}} \tag{2.4}$$

$$I_{mpp} = I_{ph} - I_0 \left(\exp\left(\frac{V_{mpp} + R_s I_{mpp}}{\gamma V_t} \right) - 1 \right) - \frac{V_{mpp} + R_s I_{mpp}}{R_{sh}} \tag{2.5}$$

Power in every point of the characteristic is given by:

$$P = VI \tag{2.6}$$

Differentiating with respect to voltage now:

$$\frac{dP}{dV} = \left(\frac{dI}{dV} \right) V + I \tag{2.7}$$

At the MPP power derivative with respect to voltage is null, therefore:

$$\frac{dI}{dV} = -\frac{I_{mpp}}{V_{mpp}} \tag{2.8}$$

Taking the derivative with respect to V of equation 2.1, the term $\frac{dI}{dV}$ can be obtained:

$$\frac{dI}{dV} = -\frac{I_0}{\gamma V_t} \left(1 + R_s \frac{dI}{dV} \right) \exp\left(\frac{V + R_s I}{\gamma V_t} \right) - \frac{1}{R_{sh}} \left(1 + R_s \frac{dI}{dV} \right) \tag{2.9}$$

Now, substituting 2.8 into 2.9:

$$\frac{I_{mpp}}{V_{mpp}} = \frac{I_0}{\gamma V_t} \left(1 + R_s \frac{I_{mpp}}{V_{mpp}} \right) \exp\left(\frac{V_{mpp} + R_s I_{mpp}}{\gamma V_t} \right) + \frac{1}{R_{sh}} \left(1 - R_s \frac{I_{mpp}}{V_{mpp}} \right) \tag{2.10}$$

Calculating I_{ph} from equation 2.3, and substituting it into 2.4 and 2.5:

$$I_{sc} = I_0 \left(\exp\left(\frac{V_{oc}}{\gamma V_t} \right) - \exp\left(\frac{R_s I_{sc}}{\gamma V_t} \right) \right) + \frac{V_{oc} - R_s I_{sc}}{R_{sh}} \tag{2.11}$$

$$I_{mpp} \left(1 + \frac{R_s}{R_{sh}} \right) = I_0 \left(\exp\left(\frac{V_{oc}}{\gamma V_t} \right) - \exp\left(\frac{V_{mpp} + R_s I_{mpp}}{\gamma V_t} \right) \right) + \frac{V_{oc} - V_{mpp}}{R_{sh}} \tag{2.12}$$

While, from the condition on the curve s slope it results:

$$-\frac{R_s}{R_{sh}} + (R_s - R_{sh}) \frac{I_0}{\gamma V_t} \exp\left(\frac{R_s I_{sc}}{\gamma V_t} \right) \tag{2.13}$$

Equations 2.10, 2.11, 2.12 and 2.13 form a set of four independent equations, with four unknowns: R_s, R_{sh}, γ and I_0. These set of equations is solved with Matlab function `fsolve`. As suggested in [8], the initial point is taken as the solution of the analytical equations, derived from some reasonable assumptions. Firstly, the approximation $\exp(V_{oc}/V_t) \gg \exp(R_s I_{sc}/V_t)$ is valid, this holds to rewrite equation 2.4 as:

$$I_0 = \left(\frac{(R_s + R_{sh} I_{sc}) - V_{oc}}{R_{sh}} \right) \exp\left(-\frac{V_{oc}}{\gamma V_t} \right) \tag{2.14}$$

Substituting it into equations 2.10, 2.12, 2.13, the following expressions can be derived respectively:

$$\frac{I_{mpp}}{V_{mpp}} - \frac{1}{\gamma V_t} \left(1 - R_s \frac{I_{mpp}}{V_{mpp}} \right) \left(\frac{(R_s + R_{sh}) I_{sc} - V_{oc}}{R_{sh}} \right) \exp\left(\frac{V_{mpp} - V_{oc} + R_s I_{mpp}}{\gamma V_t} \right) - \frac{1}{R_{sh}} \left(1 - R_s \frac{I_{mpp}}{V_{mpp}} \right) = 0 \tag{2.15}$$

$$- I_{mpp}\left(1+\frac{R_s}{R_{sh}}\right)+\left(\frac{(R_s+R_{sh})I_{sc}-V_{oc}}{R_{sh}}\right)\left[1-\exp\left(\frac{V_{mpp}-V_{oc}+R_sI_{mpp}}{\gamma V_t}\right)\right] + \frac{V_{oc}-V_{mpp}}{R_{sh}} = 0 \quad (2.16)$$

$$-\frac{R_s}{R_{sh}}+\frac{R_{sh}-R_s}{\gamma V_t}+\left(\frac{(R_s+R_{sh})I_{sc}-V_{oc}}{R_{sh}}\right)\exp\left(\frac{R_sI_s-V_{oc}}{\gamma V_t}\right)=0 \quad (2.17)$$

Further simplifications can be made now, by saying that $R_{sh} \gg R_s$, $I_{sc} \gg V_{oc}/R_{sh}$, $1/R_{sh}(1 - R_sI_{mpp}/V_{mpp}) \cong 0$ and $(V_{oc} - V_{mpp})/R_{sh} \cong 0$. According to these reasons the term $((R_s + R_{sh})I_{sc} - V_{oc})/R_{sh}$ can be simplified by I_{sc}. Equations 2.15, 2.16 and 2.17 change to:

$$\frac{I_{mpp}}{V_{mpp}}-\frac{I_{sc}}{\gamma V_t}\left(1-R_s\frac{I_{mpp}}{V_{mpp}}\right)\exp\left(\frac{V_{mpp}-V_{oc}+R_sI_{mpp}}{\gamma V_t}\right)=0 \quad (2.18)$$

$$-I_{mpp}+I_{sc}\left[1-\exp\left(\frac{V_{mpp}-V_{oc}+R_sI_{mpp}}{\gamma V_t}\right)\right]=0 \quad (2.19)$$

$$-R_s+\frac{I_{sc}R_{sh}^2}{\gamma V_t}\exp\left(\frac{R_sI_{sc}-V_{oc}}{\gamma V_t}\right)=0 \quad (2.20)$$

While equation 2.14 can be simplified too:

$$I_0 = I_{sc}\exp\left(-\frac{V_{oc}}{\gamma V_t}\right) \quad (2.21)$$

Using the value of I_{ph} calculated from 2.3 and equation 2.21, ignoring the term V_{oc}/R_{sh}:

$$I_{ph} = I_{sc} \quad (2.22)$$

Eliminating the exponential function between equations 2.18 and 2.19 holds to:

$$\frac{V_{mpp}}{\gamma V_t}-\frac{I_{mpp}}{I_{sc}-I_{mpp}}=\frac{R_sI_{mpp}}{\gamma V_t} \quad (2.23)$$

From this and equation 2.19, the approximated values of γ and R_s can be calculated:

$$\gamma = \frac{2V_{mpp}-V_{oc}}{V_t\left[\ln\left(\frac{I_{sc}-I_{mpp}}{I_{sc}}\right)+\frac{I_{mpp}}{I_{sc}-I_{mpp}}\right]} \quad (2.24)$$

$$R_s = \frac{V_{mpp}}{I_{mpp}}-\frac{\frac{2V_{mpp}-V_{oc}}{I_{sc}-I_{mpp}}}{\ln\left(\frac{I_{sc}-I_{mpp}}{I_{sc}}\right)+\frac{I_{mpp}}{I_{sc}-I_{mpp}}} \quad (2.25)$$

After computing γ and R_s equation 2.20 can be used to obtain R_{sh}:

$$R_{sh} = \sqrt{\frac{R_s}{\left(\frac{I_{sc}}{\gamma V_t}\right)\exp\left(\frac{R_sI_{sc}-V_{oc}}{\gamma V_t}\right)}} \quad (2.26)$$

Equations 2.21, 2.24, 2.25 and 2.26 can be used to set the initial values for these quantities. Starting from this point the set of nonlinear equation forming the system, 2.10, 2.11, 2.12 and 2.13, are solved with Matlab and the values of γ, I_0, R_s and R_{sh} are computed. They will then be used in the simulation with Simulink.

The panel used as reference in this work is TP240 by an Indian manufacturer Tata Solar Power, in table 2.1 its characteristics are reported [9].

Table 2.2 shows the results obtained for the calculation of the equivalent electrical circuit s elements.

Table 2.1: Characteristics of the panel used in the simulations.

Manufacturer	Tata Solar Power
Dimensions	$1667 \times 1000 \times 40$ mm
Open circuit voltage	36.5 V
Short circuit current	8.68 A
Maximum power current	8.10 A
Maximum power voltage	29.7 V
Number of series-connected cells	60
Current temperature coefficient	$3.8365 \cdot 10^{-3}$ A/K
Voltage temperature coefficient	-0.1070 V/K

Table 2.2: Parameters of the equivalent electrical circuit.

R_s	0.1772 Ω
R_{sh}	1499.4 Ω
I_0	$7.0463 \cdot 10^{-8}$ A
γ	76.2405
n	1.2707

2.3 Adjustment to Environmental Conditions

As shown before, the characteristic of the panel is strongly dependent on environmental conditions, that is the parameters can change considerably when temperature and irradiance change. Furthermore they are also dependent on output current and voltage. A lot of different mathematical models can be found in literature because the theoretical basis of some of these relations are rather weak [11]; some examples are given in [9], [10], [12], [13] and [14]. The most common representation is the one found in [14], which is also the one mainly followed in this work. According to it, the various involved quantities can be expressed as:

$$n_{oc} = n_{ref} \frac{T_{oc}}{T_{ref}} \tag{2.27}$$

$$E_{g,oc} = E_{g,ref} \left(1 - 0.0002677 \left(T_{oc} - T_{ref}\right)\right) \tag{2.28}$$

$$I_{ph,oc} = \frac{G_{oc}}{G_{ref}} \left(I_{ph,ref} + \mu_{I_{sc}} \left(T_{oc} - T_{ref}\right)\right) \tag{2.29}$$

$$I_{0,oc} = I_{0,ref} \left(\frac{T_{oc}}{T_{ref}}\right)^3 \exp\left(\frac{1}{k_B}\left(\frac{E_{g,ref}}{T_{ref}} - \frac{E_{g,oc}}{T_{oc}}\right)\right) \tag{2.30}$$

Subscripts $()_{oc}$ and $()_{ref}$ indicate respectively operating conditions and STC conditions.

The magnitude of the two resistors changes too, but not significantly enough to be considered in the simulation. Furthermore, it would add more complexity to the model and to its implementation without bringing a significant improvement in the results; they are therefore considered as constants.

With the four parameters calculated, and their adjustment to environmental conditions, it is possible to calculate a first estimation of the maximum power point given the values of temperature and irradiance, that will then be used as starting reference value in the MPP tracking system. This will allow to extract the maximum available power from the panel even if temperature and irradiance vary, controlling the panel s output voltage with the buck-boost converter.

The output current is calculated via Newton-Raphson, using equation 2.1. To do this the vector of voltage has been created taking values from 0 V to $V_{oc} + 5$ V with a step of 1 mV. For every point the iterative method is applied to calculate the current value, until the error is

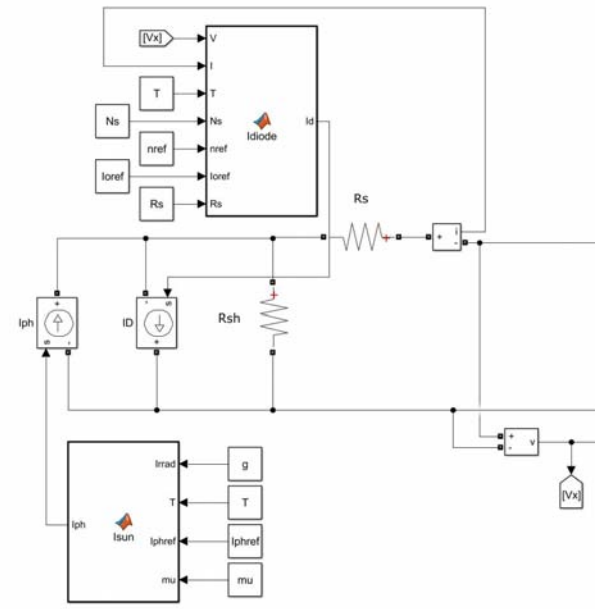

Figure 2.5: Model of the panel on Simulink

small enough, the result is saved in the vector of current and the calculation for the next point is carried out until the final point $V_{oc} + 5$ V is reached. It must be noted that the open circuit voltage moves along the voltage axis when external conditions change, all the points on the right side of V_{oc} in the actual physical state have negative current; the loop is then interrupted when the current becomes negative and its values from that point on are set to 0 A.

Current and voltage are then multiplied and power is obtained. The maximum power point is found and an index identifying its position in the power array is created, its value will then permit to find the respective values of voltage and current in the V-I characteristic at the MPP.

In figure 2.5 the model implemented in Simulink is shown. Both the diode and the photovoltaic current source are represented as controlled DC current sources; the input signal is obtained from two Matlab function blocks which include temperature, irradiance, number of series connected cells, R_s, R_{sh}, $\mu_{I_{sc}}$, reference values for I_0, I_{ph}, n and output values of voltage and current as input parameters. The reference signals are obtained by means of the previous mathematical developments.

2.4 Maximum Power Point Tracking System ans Simulations

Once the panel s model is complete, the algorithm to track down the maximum power point must be fit in the simulation. This is essential to extract the highest available power in all different weather conditions. The tracking system will produce a signal that will serve as reference for the duty cycle of the buck-boost converter. The voltage on the DC bus is now considered constant, that is the energy storage system is supposed to be able to hold it to a fixed level. This will allow to control the input voltage of the converter, i.e. the output voltage of the photovoltaic panel, changing the operation point along the current-to-voltage curve.

There are many different tracking methods, with different implementation costs, convergence speed, complexity level and range of effectiveness [15]. The most used ones are Perturb and Observe (P&O), Incremental Conductance (IncCond), Fractional Open-Circuit Voltage, Fractional Short-Circuit Current, Fuzzy Logic Control and others. They can be divided in two main categories: fixed-step sized and variable-step sized algorithms. A general overview on these methods is given in [16].

P&O is the most commonly used algorithm, the panel voltage is periodically disturbed and the corresponding output power is compared with the one of the previous perturbation. If an increment in power is noted, the next perturbation is kept in the same direction, until a decrease is recorded and the sign of the perturbation is inverted. Once the steady state is reached the system will oscillate about the MPP. This method can be implemented both with a fixed-step and variable-step size, with the last one that is usually proportional to the variation of power.

Drawbacks of this method are that the real MPP is never reached, an oscillation is generated instead and this leads to power losses. Moreover it can fail under rapidly changing atmospheric conditions as shown in figure 2.6 [15]. If environmental conditions stay approximately constant, after a perturbation ΔV the operating point will move from A to B; but if irradiance increases drastically the power curve will shift from P_1 to P_2 and now the new operating point is C. It displays a higher output power than A, the next perturbation is then going to be in the same direction as the previous one, which is clearly diverging from the MPP, and if irradiance steadily increases the perturbation will always be in the same direction. To fix this issue a three-point comparison can be made, comparing the actual power with the ones of the two previous cycles.

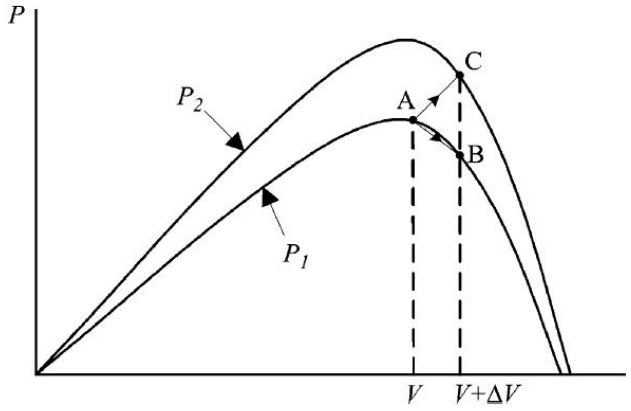

Figure 2.6: Divergence from MPP in P&O

The fractional V_{oc} method uses the fact that there s an almost linear relation between the open-circuit voltage and the voltage corresponding to the maximum power.

$$V_{mpp} \approx k_1 V_{oc} \tag{2.31}$$

where k_1 is a constant that must be determined experimentally, defining every panel, and its values are usually between 0.71 and 0.78 [15]. Once k is known, V_{mpp} can be computed measuring V_{oc}, by periodically shutting momentarily down the power converter. Of course this will result in a loss of power. Alternatively in [17] the voltage generated by the p-n junction in the condition of maximum power is claimed to be 75% of V_{oc}. In this way it is not required to shut down the converter to measure V_{oc} and a closed-loop control is enough to reach the desired voltage.

Similarly to the previous method, fractional I_{sc} calculates I_{mpp} from:

$$I_{mpp} \approx k_2 I_{sc} \tag{2.32}$$

again k_2 is a constant that must be determined through periodical measurements. In this case to measure I_{sc} an additional switch is required in order to short-circuit the panel. Both previous methods do not reach the real MPP, as 2.31 and 2.32 suggest, and involve power losses during the process.

As for fuzzy logic, it consists in three stages: fuzzification, fuzzy reasoning and defuzzification. In the first one numerical input variables are converted into linguistic variables characterised by a membership called subset, which represents each point of input subspace, called universe of discourse [3]. Two inputs are generally taken into account: $e_1 = dp/dv$ and $e_2 = d(dp/dv)/dt$, the first one gives information about the direction of the change of power and the second one

about its speed. The output is the tracking step ΔV.

$$\begin{cases} e_1 = \dfrac{dp}{dv} = \dfrac{p(z) - p(z-1)}{v(z) - v(z-1)} \\ e_2 = e_1(z) - e_1(z-1) \end{cases} \tag{2.33}$$

The fuzzy logic MPPT is performed by iterative methodology. An example of three subsets that define inputs and output are represented in figure 2.7 [3], where $e_1 \in \{negative; zero; positive\}$; $e_2 \in \{decreasing; stable; increasing\}$; $\Delta V \in \{-; 0; +\}$. In the example triangular and trape-

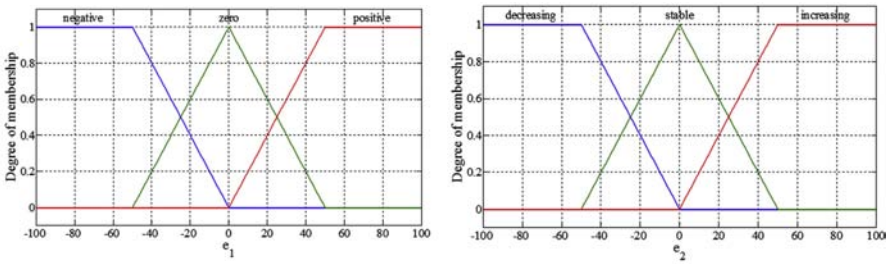

(a) Membership function for e_1.

(b) Membership function for e_2.

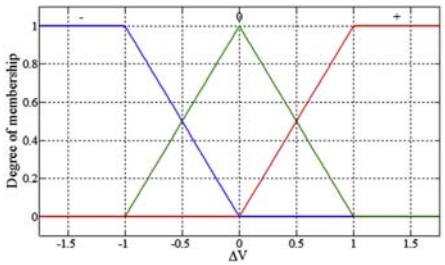

(c) Membership function for ΔV.

Figure 2.7: Membership function of inputs (2.7a and 2.7b) and output (2.7c).

zoidal functions are used, but it s also possible to use Gaussian or sigmoidal shapes, or others. In the fuzzy reasoning fuzzified inputs and outputs are mapped through if-then rules. Finally in the defuzzification the output is transformed into a numerical value to be used by the operator, and the cycle is repeated.

Fuzzy logic can operate with imprecise inputs and handle non linearities, but its complexity requires a deep knowledge of the physics and principles of the photovoltaic panel [18].

The IncCond method, which is the one chosen in this work, takes advantage of the fact that the slope of the V-P curve is null at the MPP. In facts the following relations are valid:

$$\begin{cases} dP/dv = 0 & \text{At MPP} \\ dP/dv > 0 & \text{Left of MPP} \\ dP/dv < 0 & \text{Right of MPP} \end{cases} \tag{2.34}$$

Since

$$\frac{dP}{dV} = \frac{d(IV)}{dV} = I + V\frac{dI}{dV} \approx I + V\frac{\Delta I}{\Delta V} \tag{2.35}$$

2.34 can be rewritten as

$$\begin{cases} \Delta I/\Delta V = -I/V & \text{At MPP} \\ \Delta I/\Delta V > -I/V & \text{Left of MPP} \\ \Delta I/\Delta V < -I/V & \text{Right of MPP.} \end{cases} \tag{2.36}$$

The maximum power point can thus be tracked comparing the instantaneous conductance with the incremental one, from which comes the name of the method. The flowchart in figure 2.8

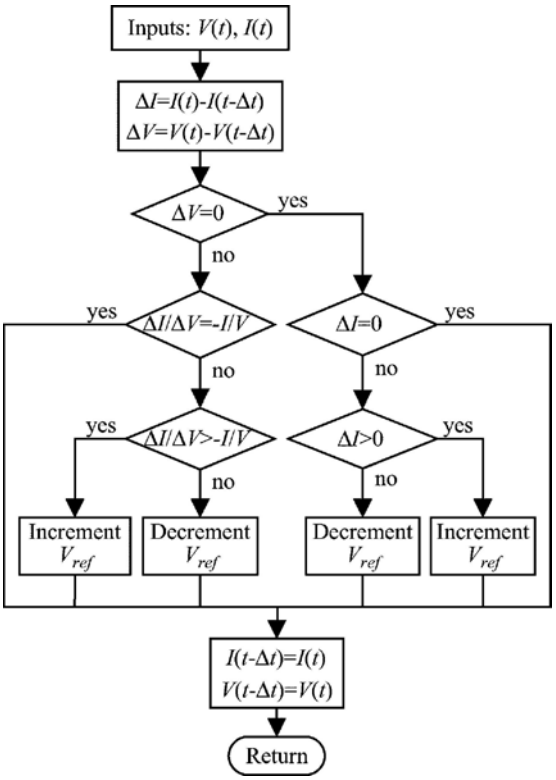

Figure 2.8: Flowchart of Incremental Conductance algorithm.

[15] describes the algorithm. V_{ref} is the reference of the panel s output voltage applied to the converter, controlled by changing its duty-cycle, it s incremented or decremented with a fixed step, properly chosen.

The rapidity with which the MPP is reached depends on the size of the step increment, its choice is a compromise between rapidity to reach the MPP and oscillations in steady state. In fact if the step size is too big it can happen that in steady state the MPP is never reached, and the algorithm keeps tracking it oscillating about the right point.

The algorithm is implemented in the simulation through a Matlab function block, whose input signals are panel s output current and voltage, the same signals delayed of a time Δt and the first value of V_{ref}. Since it s really improbable that the first condition in 2.36 is exactly satisfied, to avoid the possibility to never reach the desired point of operation a tolerance is set. It s therefore substituted with $|\Delta I/\Delta V + I/V| <$ tolerance. This leads to substitute the three conditions in the diagram where one or more variables are equalized to zero, with three different ones that take into account the consideration just made. Looking at the value that ΔI, ΔV and $\Delta I/\Delta V + I/V$ assume during the simulation, both in steady state and while tracking the MPP, the following three different values for the tolerances were chosen:

$$\begin{aligned} &|\Delta V| < 10^{-7} \\ &|\Delta I| < 10^{-7} \\ &|\Delta I/\Delta V + I/V| < 4.5 \cdot 10^{-3} \end{aligned} \tag{2.37}$$

The increment size was chosen to be 1 mV, this allows to reach the desired value quickly enough, reducing oscillations of the value of the reference voltage in a way that doesn t affect the real output voltage of the panel.

The panel and the MPP tracking system were then simulated[2]. The results are presented in figures 2.9 and 2.10, it can be seen that the algorithm is positively able to track the maximum

[2]The simulation includes also the panel's converter and its controller, which will be presented in the next chapter.

power point even when variations of environmental conditions are considered. Tests were made both with temperature and irradiance variations and the results were convincing in both cases, only an irradiance step change is shown here though, since it s the most likely to happen and the fastest too, therefore the most problematic one.

Firstly it can be noticed as V_{pv} follows its reference V_{ref}; the initial condition were set with $V_{pv} = 29$ V and $V_{ref} = 29.5$ V and after approximately 0.2 s they reach $V_{mpp} \approx 29.7$ V. Secondly, the behaviour of V_{pv} at the beginning of the simulation and after the change of irradiation at 0.25 s is a consequence of the choice of simulation solver and step size, in fact decreasing this last one the amplitude of the oscillation becomes much smaller. Last but not least the ripple in the value of V_{ref} is visible; it is also highlighted in figure 2.11 how this is very reduced and it doesn t seriously affect the dynamic of the simulation.

The MPPT system is therefore able to track the right maximum power point, calculating the right voltage reference that must be applied to the PV panel. The controller, on its side, is able to apply this reference to the panel, when variations happen a particular behaviour is displayed, that can be explained with the considerations previously made. Nevertheless after a short transitory the correct value is promptly reached.

The developed model of the photovoltaic panel is congruent with the data provided by the manufacturer, this means that the mathematical description of the model and the numerical analysis realized to calculate its parameters are an efficient representation of the real behaviour of the panel.

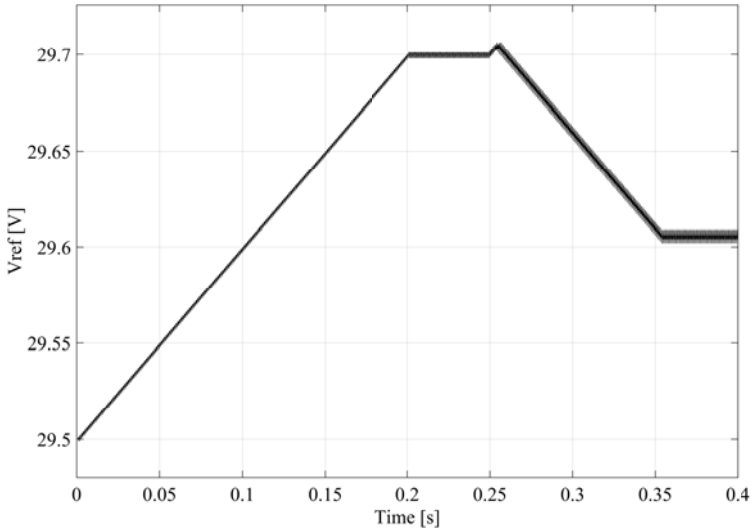

Figure 2.9: Reference output voltage of the photovoltaic panel.

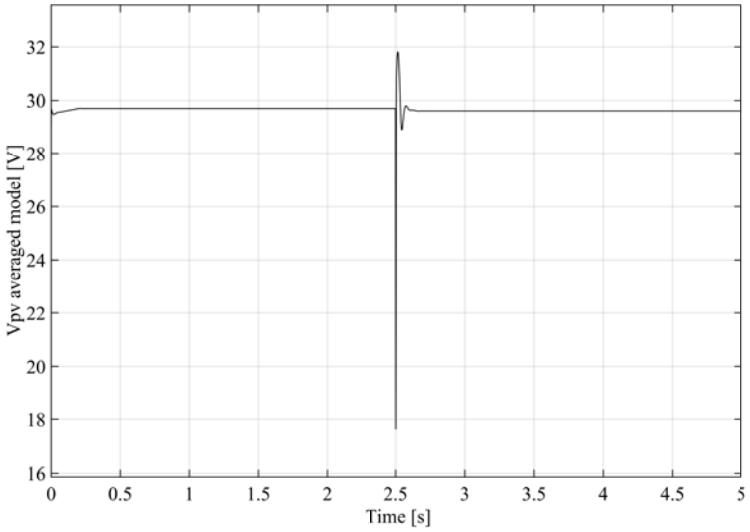

Figure 2.10: Panel s output voltage in the averaged model.

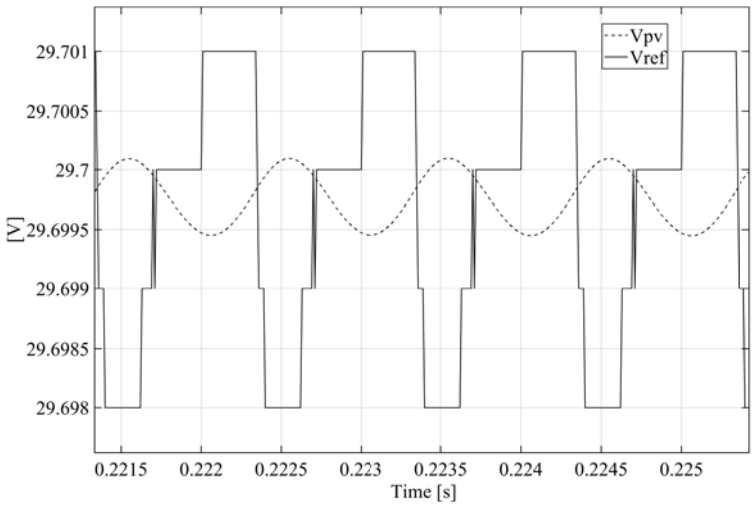

Figure 2.11: Ripple in V_{ref} and V_{pv}.

Chapter 3

DC-DC Converter for the Photovoltaic Panel

The PV panels needs a controlled dc-dc converter to implement the MMPT algoritm. A buck-boost DC-DC converter is chosen, because it will be necessary to raise the output voltage of the panel to a suitable level for the DC grid, in preparation of the connection to the AC side. The converter was firstly studied separately from the photovoltaic panel in order to understand its behaviour and the influence of the various components. In this chapter a model, and its relative control system controlling the output voltage of the DC-DC converter is initially studied, making some important considerations that will eventually be used, when the model to control the input voltage will be presented. In a first moment a formal analysis is developed, then the system is studied using parametric sensitivity analysis and from this the controller s parameters are set to a proper value.

3.1 Average Model for the Control of V_{C_o}

The circuit of the converter is shown in 3.1. It is composed by a voltage source that represents the output signals from the photovoltaic panel, a switch (commonly a MOSFET), a diode, an inductor, and a capacitor in parallel to the load. As it was specified before, in this first phase the photovoltaic panel is excluded from the model and the configuration just shown is considered.

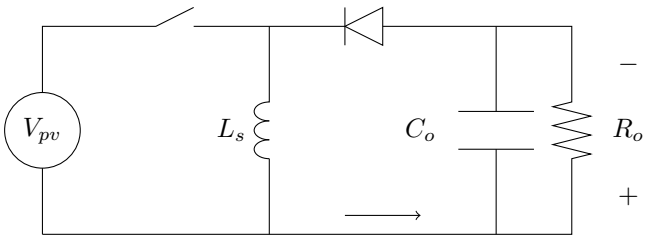

Figure 3.1: Equivalent circuit of a buck-boost converter.

This converter has two operational states: one where the switch is closed and it s conducting current, and another one when it s open. To build the average model the state variables must be identified. These are the current in the inductor and the voltage of the output capacitor. With the switch closed the input voltage is applied to the inductor, and it s charged by the input current. The diode is reverse-biased since the output voltage has a reverse polarity with respect to the input, that is a buck-boost converter is defined as inverting. The load is therefore supplied by the capacitor, that is supposed to have been previously charged and is now discharging. In

this situation the circuit is described by:

$$\begin{cases} L_c \dfrac{di_{L_c}}{dt} = V_{pv} \\ C_o \dfrac{dv_{C_o}}{dt} = -\dfrac{v_{C_o}}{R_o} \end{cases} \tag{3.1}$$

On the other hand, when the switch is open the inductor s current will keep flowing in the circuit forcing the diode in a forward-biased state. The inductor will supply the current needed by the load and will also charge the capacitor, the voltage applied to it will now be the output voltage. In this state the equations become:

$$\begin{cases} L_c \dfrac{di_{L_c}}{dt} = -v_{C_o} \\ C_o \dfrac{dv_{C_o}}{dt} = i_{L_c} - \dfrac{v_{C_o}}{R_o} \end{cases} \tag{3.2}$$

The system can be described with the typical state-space representation [20]:

$$\begin{aligned} \dot{\mathbf{x}} &= \mathbf{A}\mathbf{x} + \mathbf{B}\mathbf{u} \\ \mathbf{y} &= \mathbf{C}\mathbf{x} + \mathbf{D}\mathbf{u} \end{aligned} \tag{3.3}$$

where $\mathbf{x} = \begin{bmatrix} i_{L_c} \\ v_{C_o} \end{bmatrix}$ is the vector of the state-space variables, $\mathbf{u} = \begin{bmatrix} V_{pv} \end{bmatrix}$ is the input or control vector, $\mathbf{A}$ is the state matrix, $\mathbf{B}$ is the input matrix, $\mathbf{y} = \begin{bmatrix} v_{C_o} \end{bmatrix}$ is the output vector, $\mathbf{C}$ is the output matrix and $\mathbf{D}$ is the feedforward matrix. The output voltage of the converter is chosen now as the variable to control, in order to understand what parameters influence the response of the converter, later on the input voltage V_{pv} will be controlled instead. In the two cases they become:

Switch on

$$\begin{aligned} \mathbf{A_{on}} &= \begin{bmatrix} 0 & 0 \\ 0 & -\dfrac{1}{R_o C_o} \end{bmatrix} \\ \mathbf{B_{on}} &= \begin{bmatrix} \dfrac{1}{L_c} \\ 0 \end{bmatrix} \\ \mathbf{C_{on}} &= \begin{bmatrix} 0 \\ 1 \end{bmatrix} \\ \mathbf{D_{on}} &= 0 \end{aligned} \tag{3.4}$$

Switch off

$$\begin{aligned} \mathbf{A_{off}} &= \begin{bmatrix} 0 & -\dfrac{1}{L_c} \\ \dfrac{1}{C_o} & -\dfrac{1}{R_o C_o} \end{bmatrix} \\ \mathbf{B_{off}} &= \begin{bmatrix} 0 \\ 0 \end{bmatrix} \\ \mathbf{C_{off}} &= \begin{bmatrix} 0 \\ 1 \end{bmatrix} \\ \mathbf{D_{off}} &= 0 \end{aligned} \tag{3.5}$$

Supposing to have ideal components, the switch will be close for a time $T_{on} = dT_s$, being the duty-cycle $d = \frac{T_{on}}{T_s}$, and will be open for a time $T_{off} = (1-d)T_s$. Linearising now, all the elements in 3.4 must be multiplied by d and the elements in 3.5 by $(1-d)$, T_s is omitted since it s going to be reduced, and then they must be summed together. While averaging the different terms, the average of a product of two variables is simplified as the product of the average terms, under the assumption that their values don t vary in a perceptible way in the period T_s. Finally

the matrices describing the average model and the relative system of equations are:

$$\begin{aligned}
\mathbf{A} &= \begin{bmatrix} 0 & -\dfrac{1-d}{L_c} \\ \dfrac{1-d}{C_o} & -\dfrac{1}{R_o C_o} \end{bmatrix} \\
\mathbf{B} &= \begin{bmatrix} \dfrac{d}{L_c} \\ 0 \end{bmatrix} \\
\mathbf{C} &= \begin{bmatrix} 0 \\ 1 \end{bmatrix} \\
\mathbf{D} &= 0
\end{aligned} \tag{3.6}$$

$$\begin{cases}
\dfrac{di_{L_c}}{dt} = -\dfrac{1-d}{L_c} v_{C_o} + \dfrac{d}{L_c} V_{pv} \\
\dfrac{dv_{C_o}}{dt} = \dfrac{1-d}{C_o} i_{L_c} - \dfrac{1}{R_o C_o} v_{C_o} \\
v_{C_o} = v_{C_o}
\end{cases} \tag{3.7}$$

From the equations the circuit of the average model in figure 3.2 is derived.

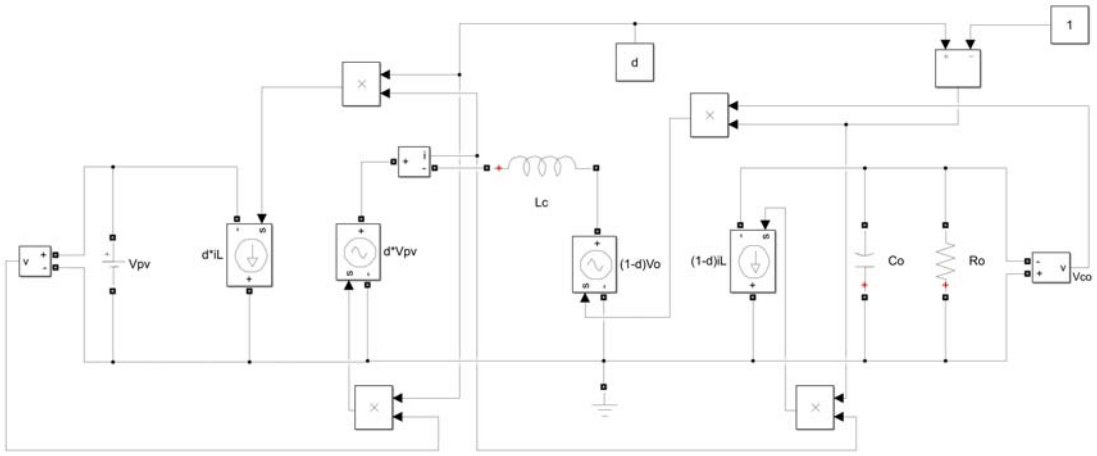

Figure 3.2: Model of the converter for the control of V_{C_o} used in the simulation.

3.2 Parameters Calculation and Simulink Implementation

To fit the converter in the simulation, the value of the components must be calculated first. To do this some constraints are imposed on input and output voltages and currents, like switching frequency and permitted ripple, range of operation. The procedure on [21] has been followed, providing some modifications to better fit it into this specific model. Firstly an approximative range of operation for V_{pv}, that is the input voltage for the converter, has been defined considering temperature variations, while its output voltage (that is the voltage applied to the capacitor) is now considered fixed (200 V). The same has been done with power, setting a nominal value; from these two parameters the nominal value for output current has been obtained with:

$$\begin{aligned}
I_o = \frac{P_o}{V_o} \qquad & P_o = \text{Nominal average output power} \\
& V_o = V_{C_o} = \text{Nominal average output voltage}
\end{aligned} \tag{3.8}$$

Consequently the equivalent load resistance R_{load} is calculated from the output voltage to current ratio. The minimum and maximum values of the duty-cycle are defined.

$$\begin{aligned} d_{min} &= \frac{V_o}{V_{pv,max} + V_o} \\ d_{max} &= \frac{V_o}{V_{pv,min} + V_o} \end{aligned} \tag{3.9}$$

The relation between average output and inductor current is:

$$I_o = I_{L_c}(1-d) = \frac{V_o T_s}{2L_c}(1-d)^2 \qquad T_s = \text{Switching period} \tag{3.10}$$

Starting from 3.10 a value is set from the fact that the inductor must be able to store enough energy in order to provide the output current during the time $T_{off} = (1-d)\,T_s$, when the switch is turned off and the output is fed, as previously said, by the inductor. The least energy is stored when the duty-cycle is equal to d_{min}, therefore combining 3.10 and 3.9:

$$L_c = \frac{R_o\,(1-d_{min})^2}{2f_s} \qquad f_s = \text{Switching frequency} \tag{3.11}$$

As the value is the minimum required to satisfy the previous condition it can be increased to make sure it is fulfilled. Similarly the value of the capacitance is calculated. A maximum acceptable ripple is set, ΔV_o, and according to this the capacitance is obtained as:

$$C_o = \frac{d_{max} V_o}{f_s R_o \Delta V_o} \tag{3.12}$$

The model is then implemented in Simulink and simulated. To validate the average model, a switched model is built too. This will take into account the ripple derived from the switching device (a MOSFET); to approve the result obtained with the average model the curve of the output voltage of the converter, that is the variable now controlled, must match the one obtained with the switched one.

Table 3.1: Converter s parameters

Parameter	Symbol	Value
Maximum input voltage	$V_{pv,MAX}$	V_{oc}
Minimum input voltage	$V_{pv,min}$	10 V
Output voltage	V_o	200 V
Switching frequency	f_s	10000 Hz
Nominal output power	P_o	P_{mpp} W
Converter inductance	L_c	0.037 H
Converter capacitance	C_o	23.586 μF
Converter resistance	R_o	166.27 Ω

3.3 Obtaining the Transfer Function for the Control of V_{C_o}

To understand the influence the components of the converter have on its response and to build a proper controller, the open-loop input to output transfer function is developed in a formal way. It is then shown though that it would be very complicated to study it from a formal point of view so a parametric analysis is carried out and some simplifications are introduced. Applying Laplace transform, the transfer function can be obtained [22]; it is needed for steady state open-loop and feed-forward control:

$$H(s) = \frac{\mathbf{Y(s)}}{\mathbf{U(s)}} = \mathbf{C}^T(s\mathbf{I} - \mathbf{A})^{-1}\mathbf{B} = \frac{V_{pv} R_o (1-d)}{C_o L_c R_o s^2 + L_c s + R_o (1-d)^2} \tag{3.13}$$

This is a second order system, this means that the closed-loop transfer function is going to be one order higher, making the control more complicated to tune. It is equal to:

$$W(s) = \frac{H(s)}{1 + H(s)C(s)} = \frac{\dfrac{R_o V_{pv}(1-d)}{C_o L_c R_o s^2 + L_c s + R_o(1-d)^2}}{1 + \dfrac{R_o V_{pv}(1-d)}{C_o L_c R_o s^2 + L_c s + R_o(1-d)^2} k_P \left(1 + \dfrac{1}{T_I s}\right)} = \tag{3.14}$$
$$= \frac{s T_I R_o V_{pv}(1-d)}{C_o L_c R_o T_I s^3 + L_c T_I s^2 + \left(R_o(1-d)^2 + R_o V_{pv} k_P (1-d)\right) T_I s + R_o V_{pv} k_P (1-d)}$$

with:

$$\begin{aligned} C(s) = k_P \left(1 + \frac{1}{T_I s}\right) &= \text{Controller transfer function} \\ k_P &= \text{Proportional constant} \\ T_I &= \text{Integral time constant} \end{aligned} \tag{3.15}$$

It is difficult to properly set a controller because of the number of parameters involved and the complexity of the transfer function. It has been chosen instead to proceed analysing the parametric sensitivity.

3.4 PI controller and parametric tuning

The control of the voltage in the buck-boost converter can be made by using the transfer function in 3.13. The dynamic of the converter is a second order system, the closed loop of block diagram generates a third order system for the PI control. From the dynamic of the converter we can check how the eigenvalues of the converter influence it.

Using the parameter in Table 3.1 the converter has the eigenvalues in $\lambda_1 = -247.244$ and $\lambda_2 = -7.748$. These real eigenvalues exhibit a first order dominant dynamic. The second eigenvalue is the most important of this particular application. A way of setting the parameters for the PI controller is by reducing the dynamic to a first order system, by knowing which of the energy storage elements has the most contribution to the second eigenvalue. The two energy storage elements are the inductance L_c and the capacitance C_o. By using the Parametric sensitivity as proposed in [23] is easy to see that the sensitivity of the second eigenvalue is mainly driven by the inductance.

Table 3.2: Parametric sensitivity analysis

Parameter	sensitivity for λ_1	sensitivity for λ_2
L_c	-0.71	0.71
C_o	1	0

The values in table 3.2 exhibit the dominance of the capacitance in the first eigenvalue. Meaning that the dynamic of the converter is mainly driven by the inductance L. The first order reduced transfer function is:

$$H'(s) = \frac{V_{pv} R_o (1-d)}{L_c s + R_o (1-d)^2} \tag{3.16}$$

where the approximated eigenvalue is $\hat{\lambda}_2 = -7.748$. The closed loop control can be done using classic PI controller in the form of:

$$C(s) = k_P \left(1 + \frac{1}{T_I s}\right) \tag{3.17}$$

where k_P is the proportional gain and T_I is the time response. The control objectives are set so a second order response are accordingly to table 3.3.

Table 3.3: PI controller s parameters

Parameter	Symbol	Value
Integral time response time	T_I	1 ms
Damping coefficient	ζ_{PI}	0.7

The eigenvalues in closed loop of the reduced model are: $\lambda_1 = -7.748$, $\lambda_2 = -7.169$ and $\lambda_3 = -0.584$.

3.5 Average Model for the Control of V_{pv}

Once the model to set the control of V_{C_o} has been understood, the one to control V_{pv} can be developed. Its behaviour is very similar, in fact again the capacitor plays an important role, allowing to neglect the inductor when computing the transfer function, reducing this way the model of one order and making much easier to set the values of k_P and T_i.

The input side of the converter is connected to the output of the photovoltaic panel and a capacitor is included to help stabilising the voltage. The structure of the model of the converter is mainly unchanged, except for the output that, while developing the model, consists of a DC voltage source with amplitude equal to V_o, which will be substituted with the output resistor and capacitor used in the first instance when the complete simulation will be run. Moreover a capacitor C_{in} is introduced in the output of the photovoltaic panel, that will help holding the voltage reducing its ripple. Its value has been chosen to be 10^{-4} F. The state variables are now the current in the inductor and the voltage of the input capacitor.

When the switch is closed the load is disconnected from the input. The voltage applied to the inductor can be expressed as:

$$L_c \frac{di_{L_c}}{dt} = v_{pv} \tag{3.18}$$

Kirchhoff s current law can be applied on the input side:

$$I_{ph} = I_D + I_{R_{sh}} + I_{R_s} = I_D + I_{R_{sh}} + C_{in}\frac{dv_{pv}}{dt} + i_{L_c} \tag{3.19}$$

$I_{R_{sh}}$ can be calculated applying Kirchhoff s voltage law:

$$\begin{aligned} R_{sh} I_{R_{sh}} &= R_s \left(C_{in}\frac{dv_{pv}}{dt} + i_{L_c} \right) + v_{pv} \\ I_{R_{sh}} &= \frac{R_s}{R_{sh}} \left(C_{in}\frac{dv_{pv}}{dt} + i_{L_c} \right) + \frac{v_{pv}}{R_{sh}} \end{aligned} \tag{3.20}$$

and can be substituted in 3.19 getting:

$$I_{ph} = I_D + \frac{R_s}{R_{sh}} \left(C_{in}\frac{dv_{pv}}{dt} + i_{L_c} \right) + \frac{v_{pv}}{R_{sh}} + C_{in}\frac{dv_{pv}}{dt} + i_{L_c} \tag{3.21}$$

From 3.21 $C_{in}\frac{dv_{pv}}{dt}$ can be isolated:

$$C_{in}\frac{dv_{pv}}{dt} = -i_{L_c} - \frac{v_{pv}}{R_s + R_{sh}} + (I_{ph} - I_D)\frac{R_{sh}}{R_s + R_{sh}} \tag{3.22}$$

Equation 3.22 together with 3.18 form the system describing the converter in the on-state of the switch:

$$\text{Switch on} \qquad \begin{cases} L_c \dfrac{di_{L_c}}{dt} = v_{pv} \\ C_{in}\dfrac{dv_{pv}}{dt} = -i_{L_c} - \dfrac{v_{pv}}{R_s + R_{sh}} + (I_{ph} - I_D)\dfrac{R_{sh}}{R_s + R_{sh}} \end{cases} \tag{3.23}$$

When the switch is open the current I_{pv} produced by the photovoltaic panel charges the capacitor C_{in}, while the inductor feeds the load. In this situation it is:

$$L_c \frac{di_{L_c}}{dt} = -V_o \tag{3.24}$$

and applying again KCL and KVL:

$$I_{pv} = C_{in} \frac{dv_{pv}}{dt} = I_{ph} - I_D - I_{rh} \tag{3.25}$$

$$\begin{aligned} R_{sh} I_{sh} &= R_s C_{in} \frac{dv_{pv}}{dt} + v_{pv} \\ I_{sh} &= \frac{R_s}{R_{sh}} C_{in} \frac{dv_{pv}}{dt} + \frac{v_{pv}}{R_{sh}} \end{aligned} \tag{3.26}$$

From 3.25 and 3.26 the equation for the voltage derivative of the capacitor can be derived:

$$C_{in} \frac{dv_{pv}}{dt} = \frac{R_{sh}}{R_s + R_{sh}} (I_{ph} - I_D) - \frac{v_{pv}}{R_s + R_{sh}} \tag{3.27}$$

Finally the system describing the converter in this state can be written from 3.24 and 3.27:

$$\text{Switch off} \qquad \begin{cases} L_c \dfrac{di_{L_c}}{dt} = -V_o \\ C_{in} \dfrac{dv_{pv}}{dt} = -\dfrac{v_{pv}}{R_s + R_{sh}} + \dfrac{R_{sh}}{R_s + R_{sh}} (I_{ph} - I_D) \end{cases} \tag{3.28}$$

The matrix forms of the two systems are:

$$\text{Switch on} \qquad \begin{aligned} \mathbf{A_{on}} &= \begin{bmatrix} 0 & \dfrac{1}{L_c} \\ -\dfrac{1}{C_{in}} & -\dfrac{1}{(R_s + R_{sh}) C_{in}} \end{bmatrix} \\ \mathbf{B_{on}} &= \begin{bmatrix} 0 & 0 \\ 0 & \dfrac{R_{sh}}{(R_s + R_{sh}) C_{in}} \end{bmatrix} \\ \mathbf{C_{on}} &= \begin{bmatrix} 0 \\ 1 \end{bmatrix} \\ \mathbf{D_{on}} &= 0 \end{aligned} \tag{3.29}$$

$$\text{Switch off} \qquad \begin{aligned} \mathbf{A_{off}} &= \begin{bmatrix} 0 & 0 \\ 0 & -\dfrac{1}{(R_s + R_{sh}) C_{in}} \end{bmatrix} \\ \mathbf{B_{off}} &= \begin{bmatrix} -\dfrac{1}{L_c} & 0 \\ 0 & \dfrac{R_{sh}}{(R_s + R_{sh}) C_{in}} \end{bmatrix} \\ \mathbf{C_{off}} &= \begin{bmatrix} 0 \\ 1 \end{bmatrix} \\ \mathbf{D_{off}} &= 0 \end{aligned} \tag{3.30}$$

and averaging in the period T_s, how it was done previously, the matrices and the model shown

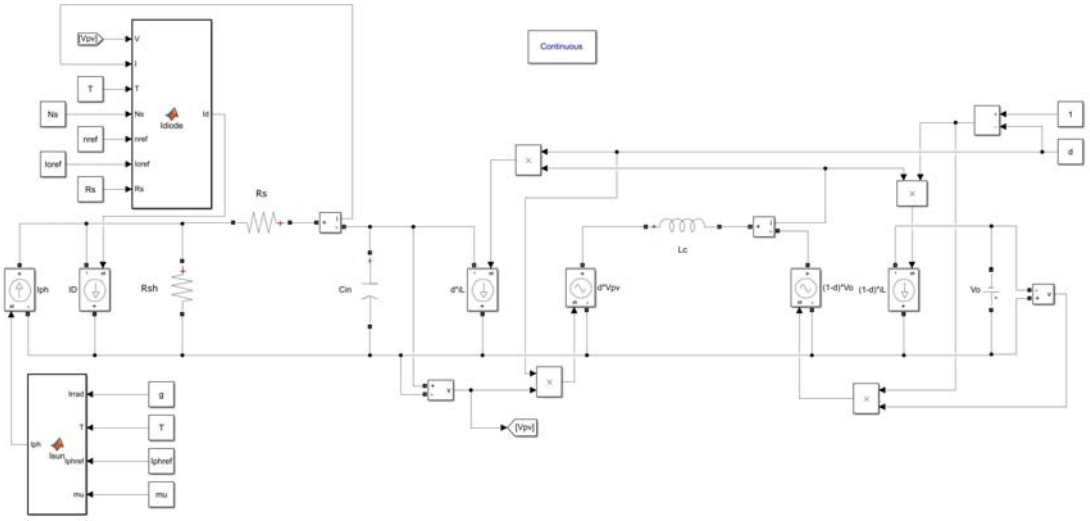

Figure 3.3: Model of the converter and of the photovoltaic panel used in the simulation

in figure 3.3 can be obtained:

$$\begin{aligned}
\mathbf{A} &= \begin{bmatrix} 0 & \frac{d}{L_c} \\ -\frac{1-d}{C_{in}} & -\frac{1}{(R_s+R_{sh})\,C_{in}} \end{bmatrix} \\
\mathbf{B} &= \begin{bmatrix} -\frac{1-d}{L_c} & 0 \\ 0 & \frac{R_{sh}}{(R_s+R_{sh})\,C_{in}} \end{bmatrix} \\
\mathbf{C} &= \begin{bmatrix} 0 \\ 1 \end{bmatrix} \\
\mathbf{D} &= 0
\end{aligned} \tag{3.31}$$

$$\begin{cases}
\dfrac{di_{L_c}}{dt} = \dfrac{d}{L_c} v_{pv} - \dfrac{1-d}{L_c} V_o \\
\dfrac{dv_{C_{in}}}{dt} = -\dfrac{1-d}{C_{in}} i_{L_c} - \dfrac{1}{(R_s+R_{sh})\,C_{in}} v_{pv} + \dfrac{R_{sh}}{(R_s+R_{sh})\,C_{in}} (I_{ph} - I_D) \\
v_{pv} = v_{pv}
\end{cases} \tag{3.32}$$

With now $\mathbf{x} = \begin{bmatrix} i_{L_c} \\ v_{pv} \end{bmatrix}$, $\mathbf{u} = \begin{bmatrix} V_o \\ I_{ph} - I_D \end{bmatrix}$, $\mathbf{y} = \begin{bmatrix} v_{pv} \end{bmatrix}$.

The same considerations done before regarding the transfer function can be applied to this situation too. A parametric sensitivity analysis is performed, with the result that the inductance L_c plays the major role in the control of the voltage V_{pv}. From this the controller is set and the input voltage of the buck-boost is controlled, that is the photovoltaic panel is operated at the MPP.

3.6 Model Implementation and Simulation

Once the converter s control system is developed, the scheme including the average model of the converter, the model of the photovoltaic panel and the Maximum Power Point Tracking System is implemented in a simulation with Simulink. To validate it the results are compared with a switched model, that is another model is created where the panel is connected to a buck boost inverter with an actual MOSFET as switching device. The same variation of irradiance previously used is imposed.

The switched model was slightly modified, considering the ripple generated by the switch in the input voltage of the converter. Since the MPPT system controls the average value of V_{pv} a filter could have been used to get rid of the undesired harmonics, but this would have introduced a delay in the system, making the comparison between the two models not reliable any longer. It was chosen instead to use a zero-order holder block to stabilise V_{ref}, holding it to a constant value for 10^{-3} s, which is the same time step of the average model; this way the voltage reference will not follow the same ripple of V_{pv} and instability is avoided.

It is important that the size of the time step, that is both for the zero-order holder and for the feedback delay of voltage and current loops, must be an integer multiple of the switching frequency, otherwise the MPPT will receive as input current and voltage measurements measured randomly during the switching period T_s. With this precaution the measurements will always be made in the same point of the switching period, as shown in figure 3.5b.

Figure 3.4 shows the comparison between the reference voltages obtained with the two models. It can be seen as the steady state values are slightly different, once the maximum power point has been tracked, this is due to the voltage ripple in the switched model that affects the MPP estimation. More important for this study is the fact that the two curves expose a very similar behaviour, with the one obtained from the switched model that is slightly slower to reach a stable condition, again because of the ripple.

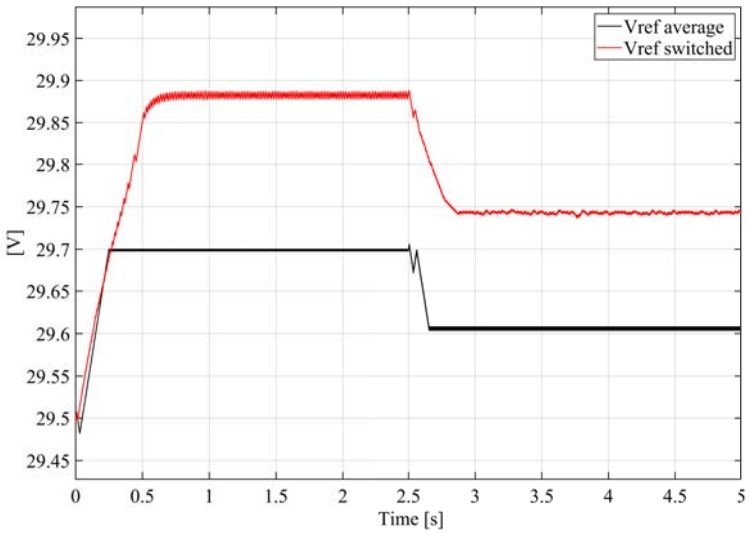

Figure 3.4: Comparison between the reference voltage in the average (black) and switched (red) models.

In 3.5a V_{ref} and V_{pv} of the switched model are shown, the reference is well tracked by the controller. Again a particular behaviour is displayed at the beginning of the simulation and when an irradiance step change is introduced, like in the average model. This is once more explained with the choice of the solver and of its time step s size.

After all these considerations, it can be stated that the average model gives a good representation of the switching device and it can be used to simulate the whole system. The reference value calculated for V_{pv} with the switched model differs from the one calculated with the averaged model because of the ripple. The last one is the one that is known to be correct, as the panel manufacturer reports [9].

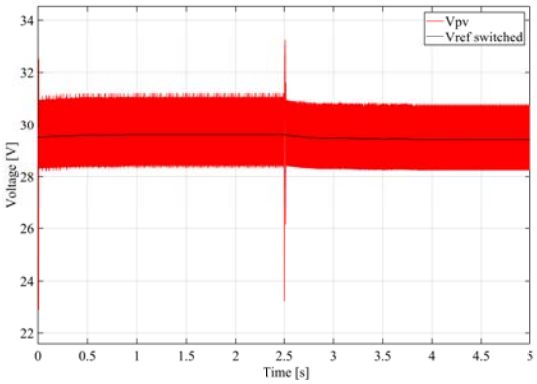

(a) Performance of V_{ref} and V_{pv} in the switched model

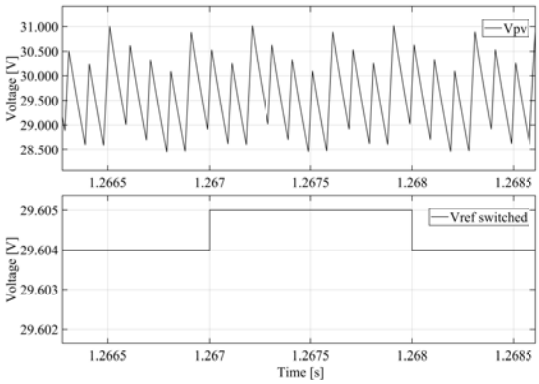

(b) Detail of 3.5a

Figure 3.5: Simulation s results of the switched model

Chapter 4

Battery

In this chapter the model of the battery is briefly presented. The battery chosen to supply the lack of power when the production of the PV panel is not enough, is a lead-acid battery. This solution is still amongst the preferred ones due to its great availability and due to the fact that it s a mature and well known technology. Other different kinds of batteries are being studied now and they seem to be able to grant better characteristics than lead-acid model, these are Nickel-metal hydride (NiMH) and Lithium-ion (Li-Ion), together with supercapacitors, whose range of operation is shown in figure 4.1 [24].

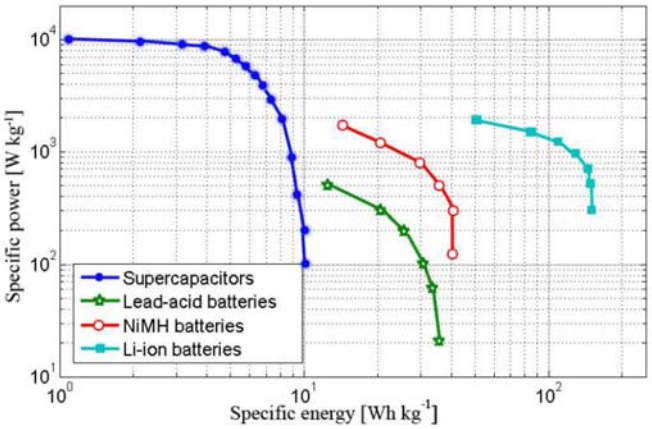

Figure 4.1: Comparison between different technologies.

The battery is connected to a buck boost converter, that will control charging and discharging operations, with the purpose of keeping the voltage on the DC bus at a fixed level. The converter has similar parameters, which are calculated in the same way previously exposed.

4.1 Battery Modelling

Firstly, it must be made clear that the aim of this work was to verify the model of the converter and its interaction with the other elements of the grid, together with their control systems. The battery model pre configured on Simulink is used, due to the complexity of building a model with passive elements that are varying in time, depending on the state of the battery. This model is composed by a controlled voltage source and a resistor representing the variable internal resistance on the battery.

The equivalent electrical circuit shows in fact a dependence on the state of charge of the battery (SOC), on its temperature and on its current intensity, with different equations for the charging and discharging states. A lot of different models have been made, with different levels of complexity taking into account different variables. Starting from the parameters given on

the data sheet by the constructor, Simulink can calculate the characteristic of the battery. The equation used and the parameters taken into account are the following, and they express the battery voltage:

Discharge Model

$$f_1(it, i^*, i, Exp) = E_0 - K\frac{Q}{Q - it}i^* - K\frac{Q}{Q - it}it + \text{Laplace}^{-1}\left(\frac{Exp(s)}{Sel(s)}0\right) \tag{4.1}$$

Charge Model

$$f_2(it, i^*, i, Exp) = E_0 - K\frac{Q}{it + 0.1Q}i^* - K\frac{Q}{Q - it}it + \text{Laplace}^{-1}\left(\frac{Exp(s)}{Sel(s)}\frac{1}{s}\right)$$

Where

E_0 is constant voltage, in V

$Exp(s)$ is exponential zone dynamics, in V

$Sel(s)$ represents the battery mode, 0 during discharging and 1 during chargin operations

K is polarization constant, in Ah^{-1}

i^* is low frequency current dynamics, in A

i is battery current, in A

it is extracted capacity, in Ah

Q is maximum battery capacity, in Ah

(4.2)

Temperature dependance is not available for lead-acid battery models, for which it s considered negligible.

The battery used for the simulation is taken from Elan s catalogue [25], and it s a 12 V, 250 Ah lead-acid battery. The characteristics are listed in table 4.1. In order to operate the

Table 4.1: Battery s electrical characteristics.

Nominal Capacity	250 Ah
Capacity at 5 hours rate (40 A)	200 Ah
Capacity at 1 hour rate (138 A)	130 Ah
Nominal Voltage	12 V

battery s converter in a better condition, it has been decided to set the output voltage of the battery to 120 V. This can be easily achieved by connecting in series 10 identical batteries. An alternative is to use a Li-Ion battery, that can reach a higher output voltage.

Chapter 5

DC to AC Converter

In this chapter the converter interfacing the DC side, with all the parts presented until now, and the AC grid is presented. It is a single phase, NPC (Neutral-Point-Clamped) VSC (Voltage-Sourced Converter) with a Phase-Locked Loop (PLL). The model was made by Sigurd Strømsem, who presented a detailed analysis of the converter in his master s thesis. His work is focused on the analysis of the linear and non-linear behaviour of the PLL under fault conditions, and together with this one they are part of a wider project. Hence the theory of the converter, of the PLL and of the controller is here briefly explained, in order to get the essential information that will be used to get a complete model.

The converter is connected to the DC link, therefore its input voltage is the output voltage of the buck-boost converter and of the battery, V_o.

The control of the converter is performed in the rotating dq-frame, where the AC signals are transformed into DC values, allowing the use of the classic PI control strategy. The dq-frame is usually obtained in three phase systems representing its signals with space phasors. These can be decomposed into two components, one real and one imaginary (Clark transformation) in a stationary cartesian system called $\alpha\beta 0$. Consequently the rotating signals can be decomposed in a system rotating with angular speed ω (Park transformation) [26]. For a single phase system the stationary reference system $\alpha\beta 0$ is obtained delaying the signal of $\pi/2$ rad, creating a fictional one, the transformation from $\alpha\beta 0$ to dq is then performed by multiplying all the signals by $e^{-\jmath\theta}$.

When the dq-system is rotating with the same frequency of the AC-side signals, that is $\omega = \omega_0$, active and reactive power are dependent only on I_d, projection of the current on the d-axis, and I_q, current projection on the q-axis, respectively. This simplifies greatly the control of the converter but, on the other hand, a system that tracks the frequency of the AC grid and corrects the one of the converter s AC signals is required. This task is performed by the PLL.

It must be studied how the MPPT system, the PLL, the controller of the battery and the power control of the DC/AC converter interact not only in steady-state operating conditions but also during fault conditions, to verify that the stability of the system is not compromised.

5.1 Model of the Converter

As said before, this is a VSC since the DC-side voltage is constant and the direction of the power flow is thus determined by the polarity of the DC current. A NPC converter is chosen because it can make a better use of the DC voltage: the output varies between V_o, 0 and $-V_o$; moreover it can offer a less distorted synthesized AC voltage [27]. The converter is interfaced with the grid through an inductor, represented by a resistance R_s and an inductance L_s, which acts as a filter ensuring a low-ripple AC-side current (in some cases the load or the AC side itself embeds the reactor and no external RL branch is needed).

First of all, the averaged model of the controller is obtained, on the assumption that the converter behaves ideally, therefore power is transmitted from one side to the other without

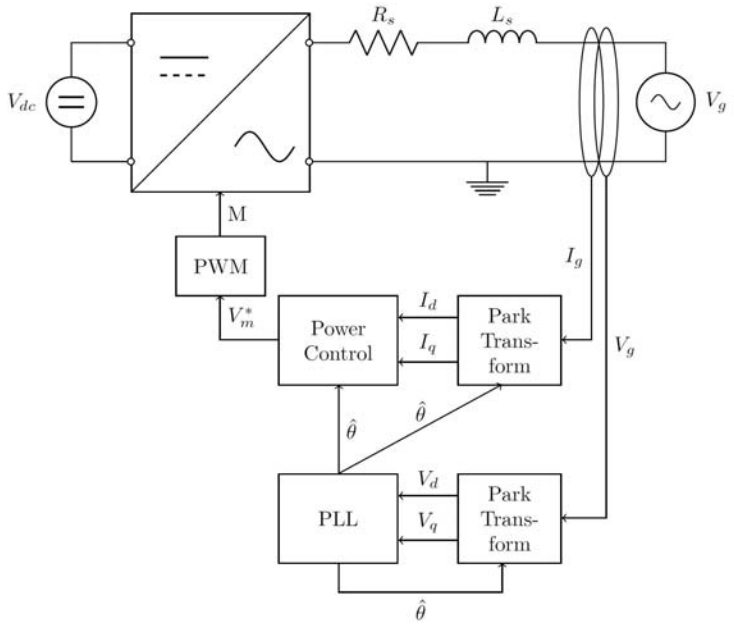

Figure 5.1: Scheme of a single-phase voltage-sourced converter.

losses in the switching devices. The following relations are valid:

$$\begin{aligned} P_{ac} &= P_{dc} \\ V_{ac} &= V_{dc}(2d-1) \\ I_{dc} &= I_{ac}(2d-1) \end{aligned} \tag{5.1}$$

with d duty-cycle of the converter, V_{dc} and I_{dc} input voltage and current on the DC side, V_{ac} and I_{ac} output voltage and current on the AC side.

Operating the converter with PWM technique it is $m = (2d-1)$ [28]. This technique controls the switching period of the switches by the comparison of two signals: one called carrier, which is generally a triangular wave with high frequency (in the order of kHz) and a modulating signal with similar characteristics of the one to reproduce; in this case the modulating signal is a sinusoidal wave with the desired frequency [29]. The ratio between modulating s and carrier s amplitude is m, and the relations in 5.1 can be rewritten as [30]:

$$\begin{aligned} V_{ac} &= mV_{dc} \\ I_{dc} &= mI_{ac} \end{aligned} \tag{5.2}$$

Applying Kirchhoff s voltage law between the converter and the grid voltage V_g:

$$L_s \frac{di_{ac}}{dt} = V_{ac} - R_s i_{ac} - V_g = mV_{dc} - R_s i_{ac} - V_g \tag{5.3}$$

Applying the $\pi/2$ delay to get the signal in the $\alpha\beta$ reference system and then Park transformation to 5.3, the equations in the dq-frame are obtained:

$$\begin{cases} L_s \dfrac{di_{ac,d}}{dt} = L_s \omega(t) i_{ac,q} + V_{ac,d} - R_s i_{ac,d} - V_g \\ L_s \dfrac{di_{ac,q}}{dt} = -L_s \omega(t) i_{ac,d} + V_{ac,q} - R_s i_{ac,q} \end{cases} \tag{5.4}$$

The system in 5.4 represents the particular, and desired, case when the rotating speed of the dq-system ω is the same one of the AC-grid signals ω_0 and the grid voltage lies on the d-axis, therefore $V_{g,q} = 0$.

Table 5.1: Values of the parameters of the VSC converter.

AC Grid Peak Voltage, V_s	120 V
AC Grid Frequency, f_{grid}	60 Hz
AC Grid Line Resistance, R_{grid}	0.15 Ω
AC Grid Line Inductance, L_{grid}	0.002 H
DC Grid Voltage, $V_o = V_{DC}$	200 V
VSC Filter Resistance, $R_{s,conv}$	0.15 Ω
VSC Filter Inductance, L_s	0.012 H

5.2 Phase-Locked-Loop

In order to have the grid voltage lying on the d-axis, it must be that the dq-frame is rotating with the same angular speed as V_g itself and that its phase with respect to the stationary reference system is the same of V_g. This can be obtained by measuring V_g, applying the transformation to dq coordinates using an estimation of the angle between the stationary and rotating systems $\hat{\theta}$, then regulating to zero trough a PI controller the component in quadrature of the grid voltage. This is called Synchronous Reference Frame (SRF) PLL [31]. The correction on the velocity of the dq-system is then applied and a new estimation of it is obtained; integrating the angular speed the new estimation on $\hat{\theta}$ is got and it s fed to the transformation block from $\alpha\beta$ to dq.

As said before, for a single phase system it is:

$$\begin{pmatrix} V_\alpha \\ V_\beta \end{pmatrix} = \begin{pmatrix} V_s \cos(\omega t) \\ V_s \sin(\omega t) \end{pmatrix} \tag{5.5}$$

and the following relations are valid:

$$\begin{aligned} V_{dq} &= V_{\alpha\beta} e^{-\jmath\hat{\theta}} \\ V_{dq} &= \begin{pmatrix} \cos(\hat{\theta}) & \sin(\hat{\theta}) \\ -\sin(\hat{\theta}) & \cos(\hat{\theta}) \end{pmatrix} V_{\alpha\beta} \end{aligned} \tag{5.6}$$

Substituting now 5.5 into 5.6:

$$V_{dq} = \begin{pmatrix} V_d \\ V_q \end{pmatrix} = \begin{pmatrix} V_s \cos(\omega t)\cos(\hat{\theta}) + V_s \sin(\omega t)\sin(\hat{\theta}) \\ -V_s \cos(\omega t)\sin(\hat{\theta}) + V_s \sin(\omega t)\cos(\hat{\theta}) \end{pmatrix} = \begin{pmatrix} V_s \cos(\hat{\theta} - \theta) \\ -V_s \sin(\hat{\theta} - \theta) \end{pmatrix} \tag{5.7}$$

It is easy now to see how V_q must be regulated to zero in order to get a correct phase prediction.

The following regions are defined: $\Omega_{hold-in}$ is the region of frequency difference where the PLL can maintain a locked state, that is it s correctly synchronised, assuming the signal was initially synchronised; $\Omega_{pull-in}$ is the range of initial frequency differences where the PLL is able to lock to a specific signal; a cycle slip occurs when the output of the phase-locked loop is incorrect, for instance if a phase shift of 2π is produced; $\Omega_{lock-in}$ is the range of initial frequency deviation where the PLL doesn t exhibit cycle slips.

In the work developed by Sigurd... is shown that the SRF-PLL can lead to instability when particular initial conditions are satisfied, however these are exceptional cases and can be ignored. The system is consequently stable, considering both its linear and non-linear behaviour, and $\Omega_{hold-in} = \Omega_{pull-in} = \mathbb{R}^2$. As for the calculation of the lock-in range an analytical estimate was followed from a PhD thesis [32].

5.3 Power Control

Moving to the $\alpha\beta$ reference system the power is preserved[1]. Expressing the apparent power S as a function of dq signals:

$$\begin{aligned} S &= V_{\alpha\beta} I^*_{\alpha\beta} = (V_\alpha + \jmath V_\beta)(I_\alpha - \jmath I_\beta) = (V_d + \jmath V_q)e^{\jmath\theta}(I_d - \jmath I_q)e^{-\jmath\theta} \\ &= (V_d I_d + V_q I_q) + \jmath(V_q I_d - V_d I_q) = P + \jmath Q \end{aligned} \tag{5.8}$$

[1] In this situation only. For a three phase system there's a factor of 1.5

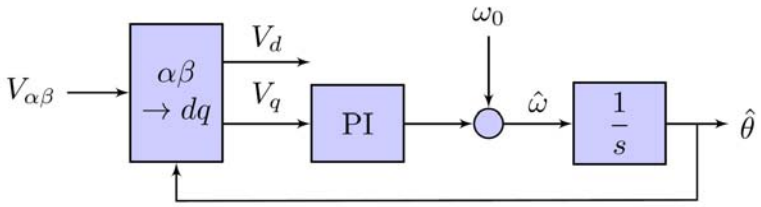

Figure 5.2: Control structure for a SRF-PLL.

Therefore:

$$P = V_d I_d + V_q I_q \tag{5.9}$$
$$Q = V_q I_d - V_d I_q \tag{5.10}$$

If the phase angle and frequency are well tracked $V_q = 0$ and:

$$P = V_d I_d \tag{5.11}$$
$$Q = -V_d I_q \tag{5.12}$$

From 5.11 and 5.12 the reference values for I_d and I_q can be obtained, setting the desired output active and reactive power. It is also clear why we want to operate in this condition, the power control is much simpler than the general case since P and Q are dependent only on I_d and I_q respectively [33].

From the system of equations 5.4 two PI controller have been set, one for the d-axis and one for the q-axis. It can also be seen that the two axes are dependent one from another, due to the presence of the term $L_s\omega(t)i_{ac,q}$ on the first and $L_s\omega(t)i_{ac,d}$ on the second one. Therefore, besides supposing that the PLL is correctly tracking phase and frequency, a further simplification can be made: by neglecting the time delay of the dynamic of the switching devices and of the current sampling, these two terms can be subtracted, decoupling the axes and obtaining two identical ones. This will allow to tune the PI controller identically.

The previous assumptions are very realistic, in fact the weaker one is that on the PLL, because of non linearities and load variations that can impose a big enough step change in the input signals, dragging it out of $\Omega_{lock-in}$ or even $\Omega_{hold-in}$.

Chapter 6

Results and Discussion

Here the results of the simulation are reported and analysed.

6.1 Panel Model and MPPT

It was shown previously how the model of the photovoltaic panel can describe with enough accuracy its behaviour, figures 2.2 and 2.3 are obtained simulating the equivalent circuit imposing different values of irradiance and temperature.

The maximum power point system is able to track the right voltage in order to operate the panel correctly. The ripple introduced is minimal and it s not affecting the converter control system as shown in 2.11.

6.2 Converter Model

Due to the complexity of the system and to the dominant dynamic of one of the eigenvalues, the control system of the converters included in the work was tuned starting from their reduced model. In this situation the behaviour is mainly driven by the inductance.

Figure 6.1 shows the results obtained for the control of V_o, where the averaged model and the switched one are compared. The averaged model brings a good representation of the real device and the assumption on the control system is reasonable: in fact the correct value is properly tracked, even when sudden step changes are introduced.

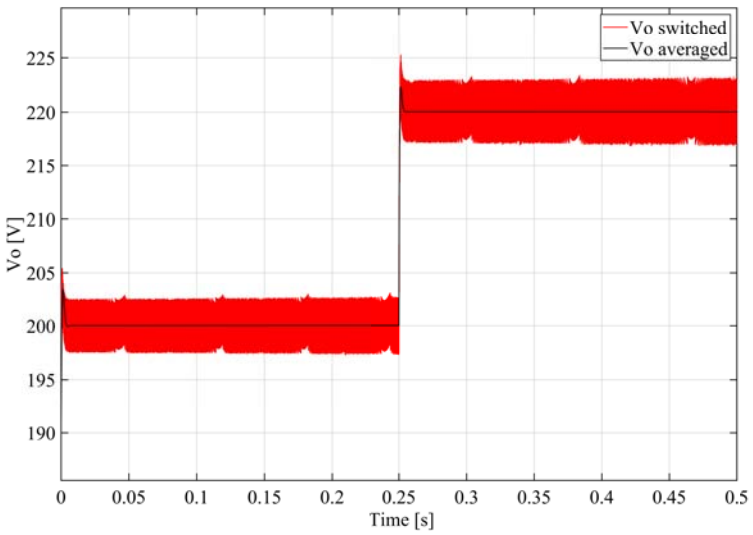

Figure 6.1: Comparison between the control of V_o in the averaged and switched models.

Some considerations must be made for what concerns the control of V_{pv}. It was previously verified in figure 2.10 that due to the choice for the solver time step a momentary instability is induced in the output voltage of the PV panel. This is also explained from the fact the the change was produced by a variation of the irradiance, which mainly affects the current generated by the panel. With the simplifications made on the transfer function, only the inductance is taken into account. Because of that the controller is subjected to higher instability when the current changes, the inductance in fact plays the main role in the dynamics of the current. This, together with the choice of the size of the time step of the solver, explains this behaviour.

The same behaviour is in fact exposed also in the switched model, as it s shown in figure 6.2 where a change of irradiance is induced at time $t = 2.5$ s. This once more validates the accuracy of the averaged model. Also the reference voltage in the two models behaves identically, excluding an error induced by the ripple due to the switching device, figure 3.4. Figure 6.3 shows the tracking of the reference voltage in the switched model, while figure 6.4 the one in the averaged model. These simulations confirm the legitimacy of using an averaged model to simulate the response of the subsystem composed by the PV panel, its converter and the MPPT algorithm. Changes of irradiance, or general changes in operating conditions, are detected efficiently by the MPPT system and a consequent change in the voltage is imposed and tracked correctly.

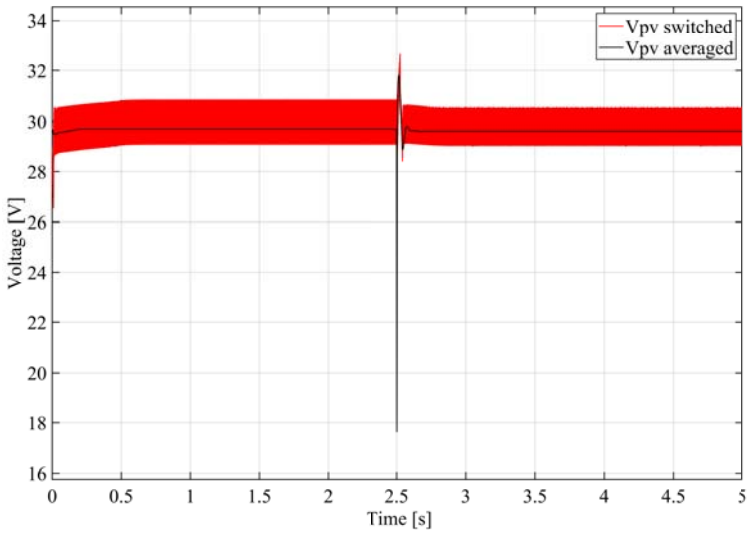

Figure 6.2: Comparison between the controlled output voltage of the photovoltaic panel, V_{pv}, in the two models.

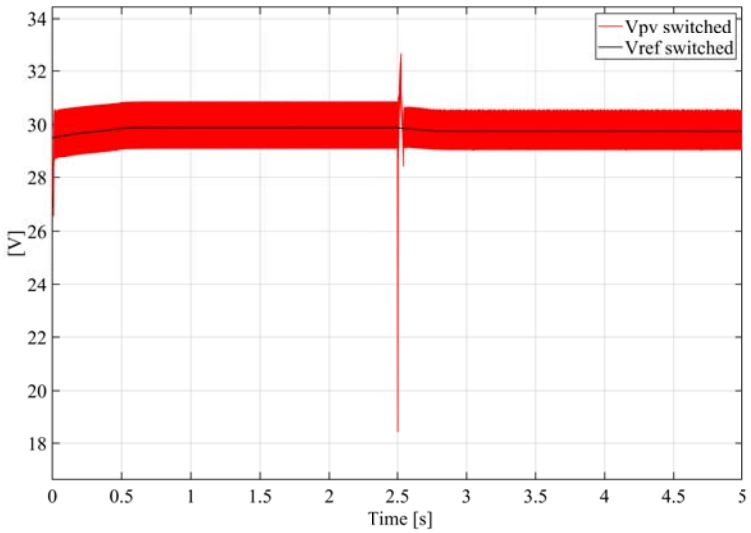

Figure 6.3: Comparison between the reference and the output voltage ot the PV panel in the switched model.

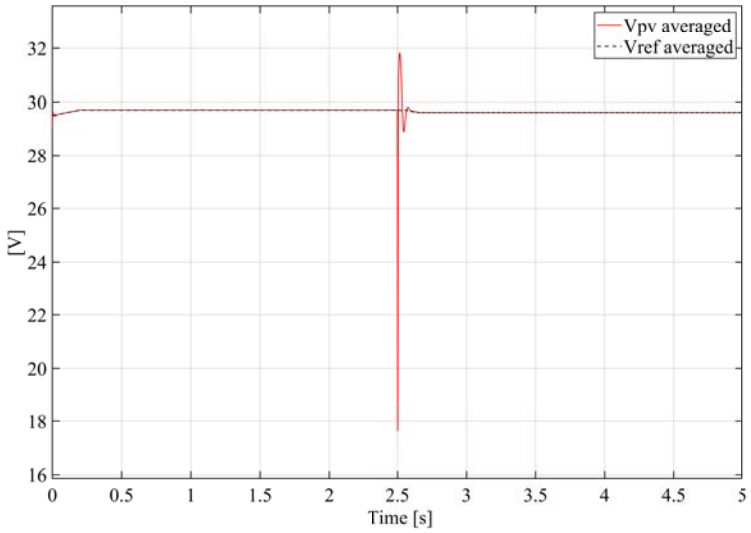

Figure 6.4: Comparison between the reference and the output voltage ot the PV panel in the averaged model.

Finally it can be stated that the averaged model is suitable for the simulation of the converter, with the previous assumptions driven by this particular configuration. Nevertheless a situation where the main role in the control of the converter is played by the inductance is something that is likely to happen, this particular case can therefore be representative of a more general condition. Furthermore the non-linearities introduced by the MPPT and by the model of the photovoltaic panel don t affect the dynamic and precision on the averaged model and its controller.

6.3 Battery

The battery is one of the most problematic components when it comes to model and simulate it. Its behaviour is in fact strongly non-linear and, even though the electrical model can provide a good representation, its dynamic is difficult to reproduce.

To simplify the model it has been chosen to use the one available on Simulink. Here the results of some simulations are reported. Again the effect of current instability are visible right before a steady state condition is reached.

Figure 6.5 reports the result of a simulation where the panel and the battery were connected to a load represented by an equivalent resistance, appositely chosen to absorb less power than the one produced by the PV panel. It is visible how the exceeding amount of power is stored in the battery, the output current of the battery s converter is in fact negative, and same goes for its power. The DC line voltage is held constant by the battery and the panel is allowed to produce the maximum available power.

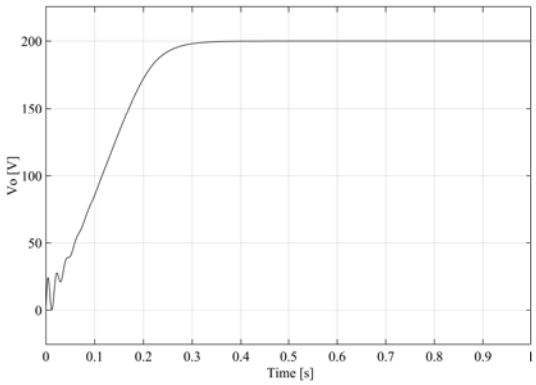

(a) DC line voltage.

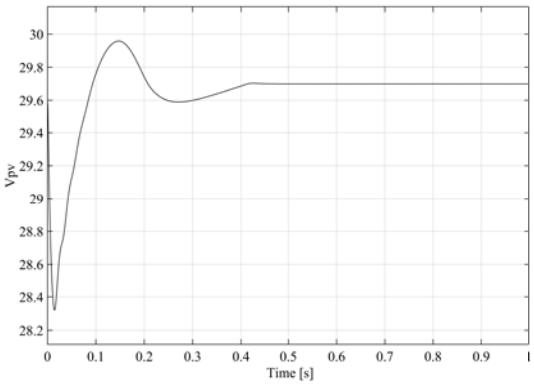

(b) Pv panel voltage.

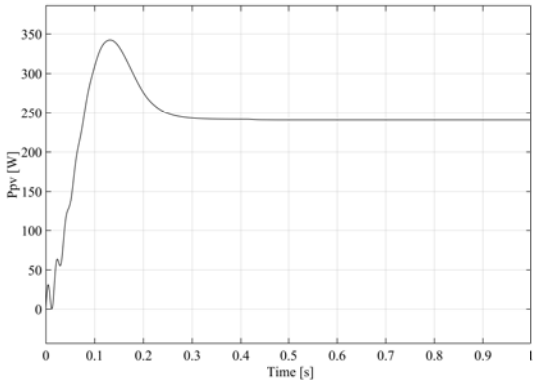

(c) Pv panel generated power.

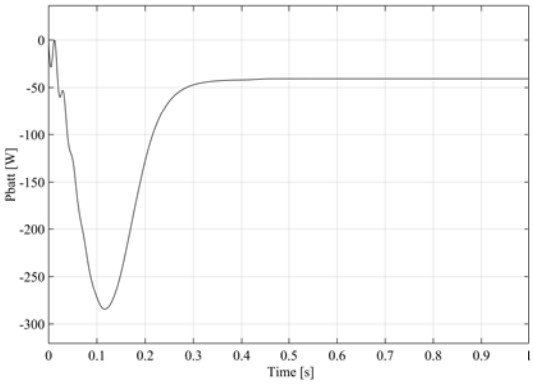

(d) Battery generated power.

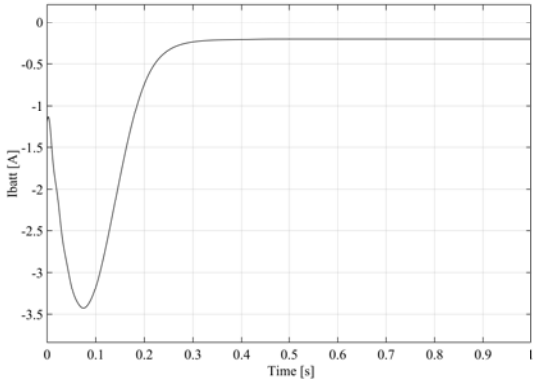

(e) Battery current input in the DC line.

Figure 6.5: Simulation results with $R_{load} = 200$, $P_{load} = 200$.

Figure 6.6 shows the results of a similar simulation, where the load was requiring a higher power, which was supplied by the battery. Again the DC voltage is kept at the desired value

and the panel works in the MPP.

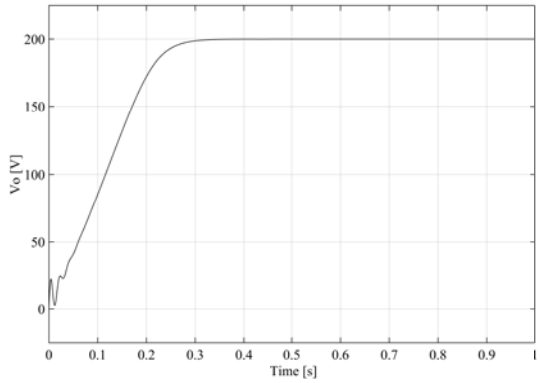

(a) DC line voltage.

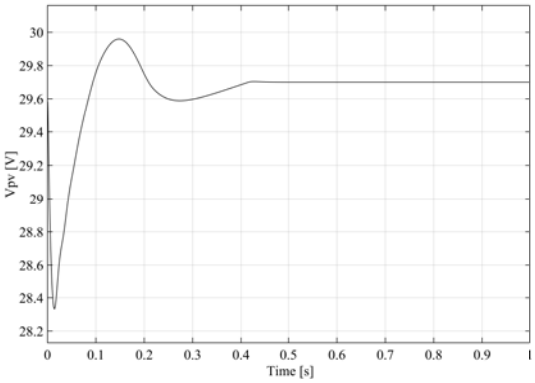

(b) Pv panel voltage.

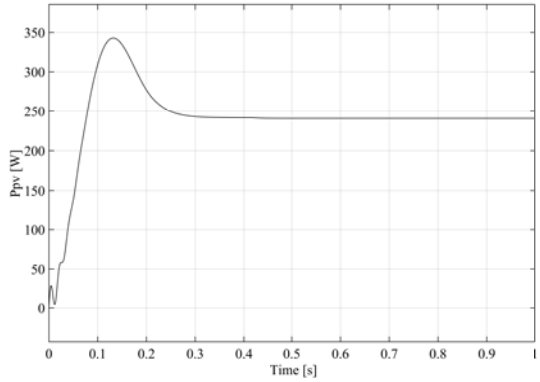

(c) Pv panel generated power.

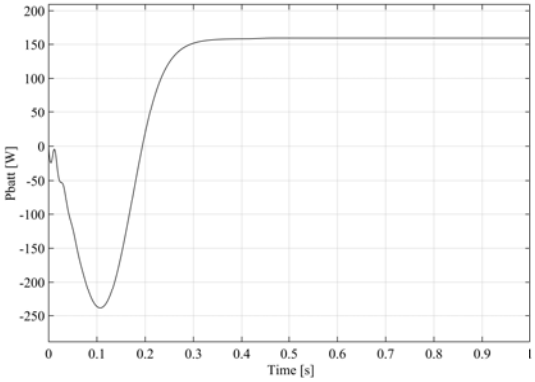

(d) Battery generated power.

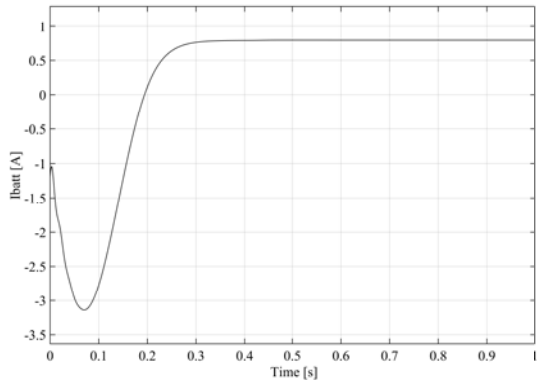

(e) Battery current input in the DC line.

Figure 6.6: Simulation results with $R_{load} = 100$, $P_{load} = 400$.

Finally in figure 6.7 the same quantities are reported in the same condition as the first simulation , but with a change in the irradiance of $\Delta g = -500$ kW/m^2. After some oscillations the value of V_0 is brought to 200 V, V_{pv} is tracking successfully the optimal value of the voltage and the battery goes from absorbing power from the panel to supplying it.

Figure 6.8 reports a detail of 6.7c and 6.7d, showing how the battery provides to the load exactly the missing power.

The model including the battery and all the other elements presented before is already very complicated, even if the DC to AC converter has still to be added. It takes into account the non linearity of the photovoltaic panel model and of the battery model, with current and voltage generated that are function of the operating conditions and of the current and voltage in the

DC line. However the results obtained simulating different situations represent with a good approximation the real behaviour of this system for this reason the model can be used properly to tune the different control systems and to predict and study its response.

6.4 DC to AC converter

As said before, the DC/AC converter was taken by the work carried on in parallel by Sigurd Strømsem. The converter behaviour is shown in the following figures, 6.9 and 6.10. A step in the active power reference was included, it is well tracked by its controller and as a consequence the output current on the AC side is reduced in amplitude.

Figure 6.11 shows how the step superimposed on the controller doesn t affect the PLL. It is not visible indeed a variation in the estimation of ω_0, and V_q is null during the time of the simulation.

When the converter was implemented in the complete simulation, it resulted in a critical situation as figure 6.12 reports. The simulation was carried out with the same parameters as in the previous ones, with the only difference that the change in the irradiance value is imposed later in order to give enough time to the converter to reach a stable condition. The instability displayed at the beginning of the simulation and when the change of irradiance is induced at time $t = 1.5$ s is now affecting the stability of the PLL. It is probable that when a sudden change leads the operating condition far from steady state operation, this induces cycle slips in the PLL. The converter isn t therefore synchronised with the grid frequency any more, this brings instability on the DC side too.

After some time though, the PLL is able to lock-in and the correct voltage values are tracked. A quite strong AC component is introduced in the DC line by the model of the DC/AC converter, as it is shown in figure 6.13. This oscillation contributes to the difficulty of the controllers to stabilise their reference signals, amplifying the transitory at the beginning of the simulation and at $t = 1.5$ s, when the irradiance changes. The sinusoidal component in the voltage can not be eliminated by PI controllers, this is why the oscillation is present in steady state regime.

For what concerns the power, figure 6.14 presents the evolution of active and reactive power. It can be immediately noticed that the active power is negative, when the reference was positive. This is because the buck-boost is an inverting converter, which means that it inverts the polarity of the voltage from the input to the output. This is not a problem since the aim of these simulations is to verify the stability of the system, the fact that the output power is seen as negative is only because of the choice of references in the AC side. To fix this issue it is enough to use a non inverting buck-boost, that adds a switching device but allows to keep the same polarity of the voltage. The relations of the inverting and non inverting buck-boos controller are the same.

Nevertheless it is visible that the same considerations made for V_o and V_{pv} are valid: after the transitory voltages reach their nominal values and the reactive power decreases to zero.

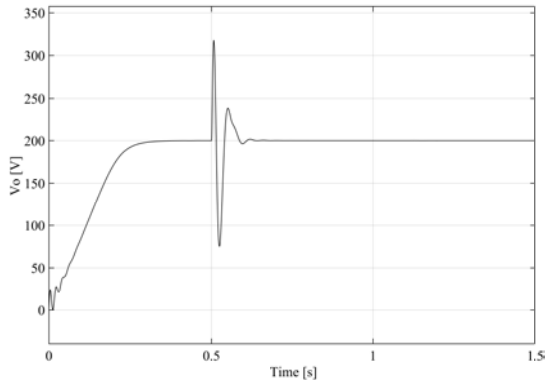

(a) DC line voltage.

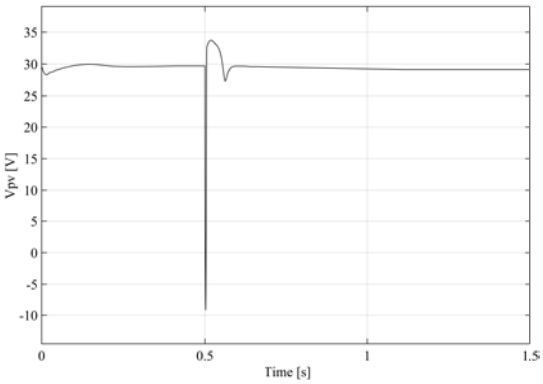

(b) Pv panel voltage.

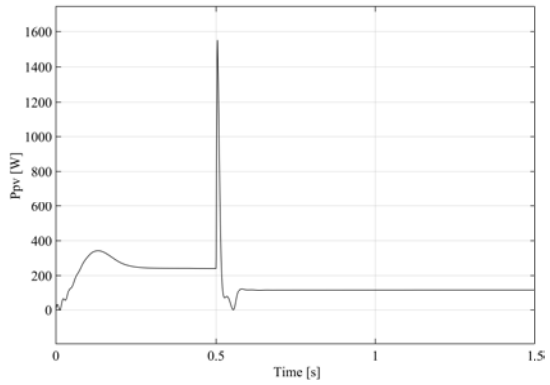

(c) PV panel generated power.

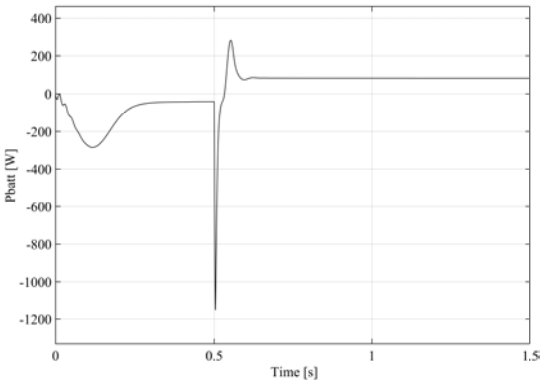

(d) Battery generated power.

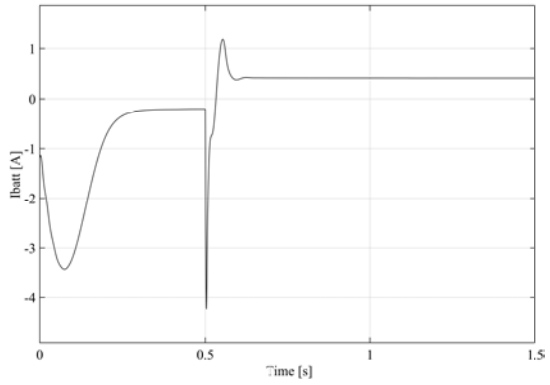

(e) Battery current input in the DC line.

Figure 6.7: Simulation results with $R_{load} = 200$, $P_{load} = 200$, $\Delta g = -500$ kW/m^2.

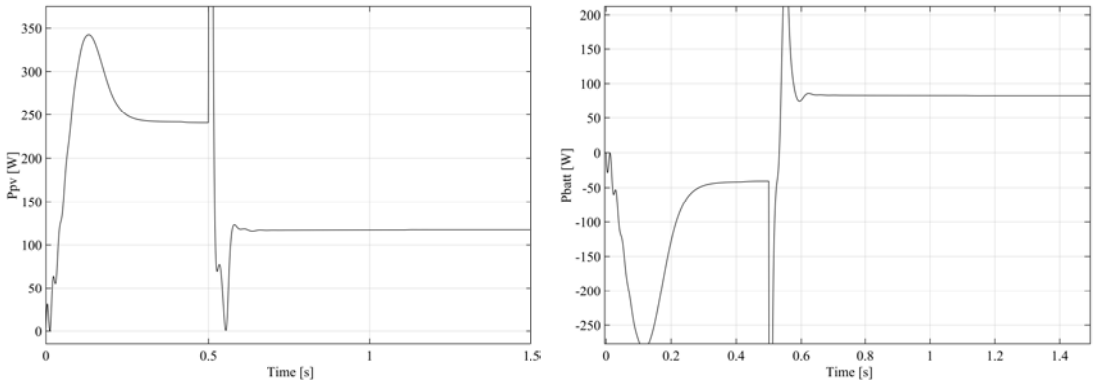

(a) PV panel generated power, detail.

(b) Battery generated power, detail.

Figure 6.8: Detail of the power balance in the last simulation.

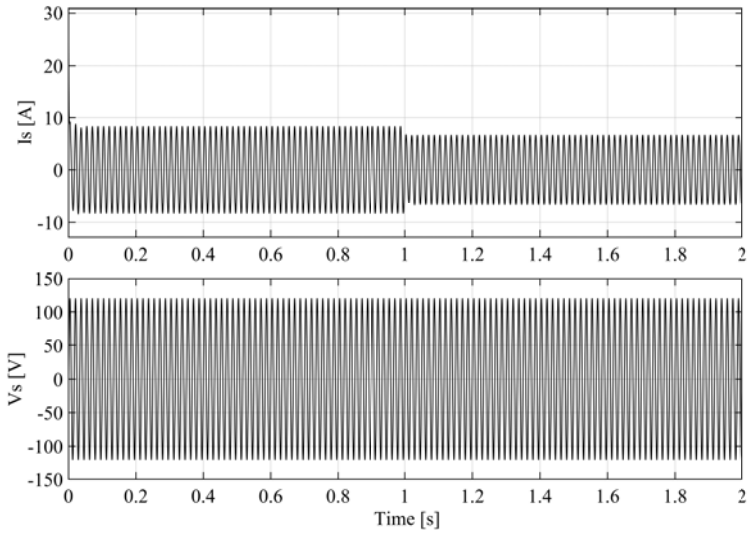

Figure 6.9: Output voltage and current of the converter in the stand-alone simulation.

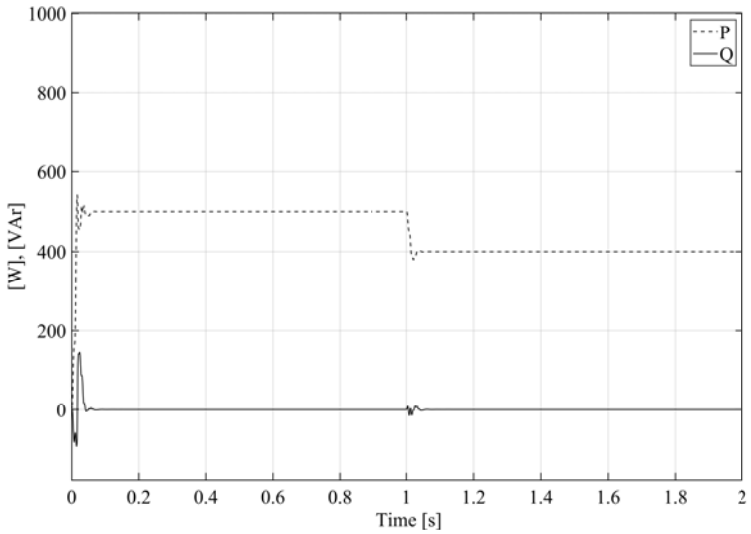

Figure 6.10: Output active and reactive power of the converter in the stand-alone simulation.

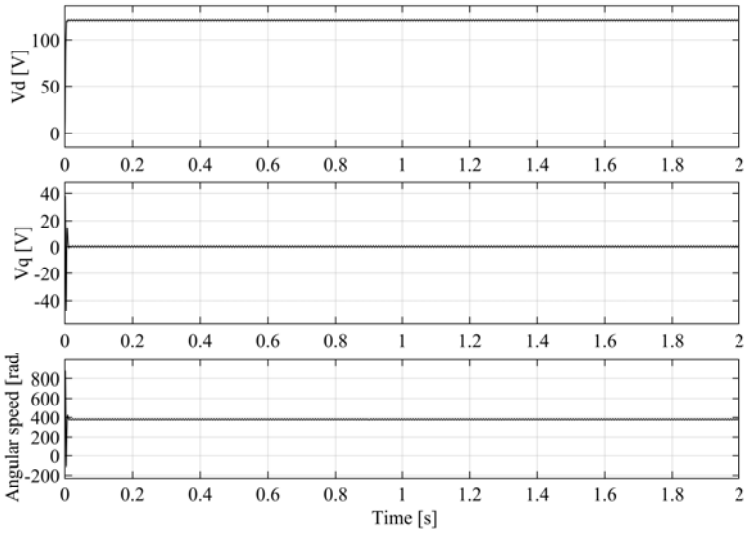

Figure 6.11: d and q components of the voltage of the converter and estimation of ω_0 in the stand-alone simulation.

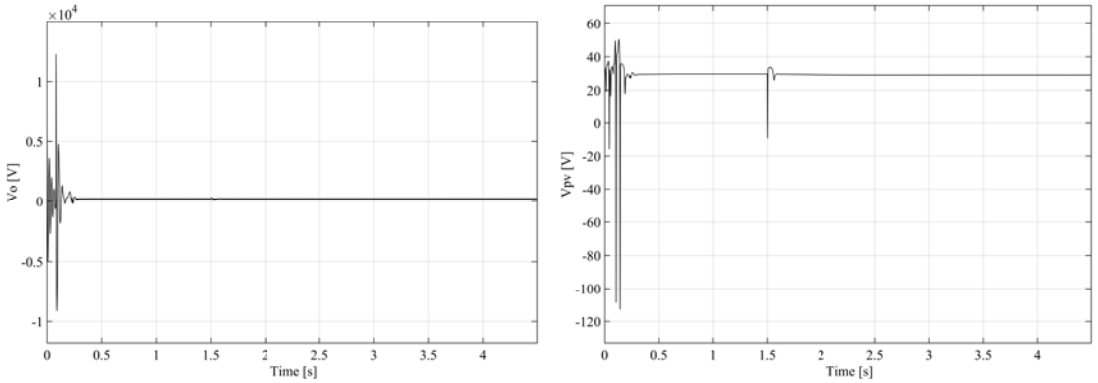

(a) DC line voltage.

(b) PV panel voltage.

Figure 6.12: Voltage profiles in the complete simulation.

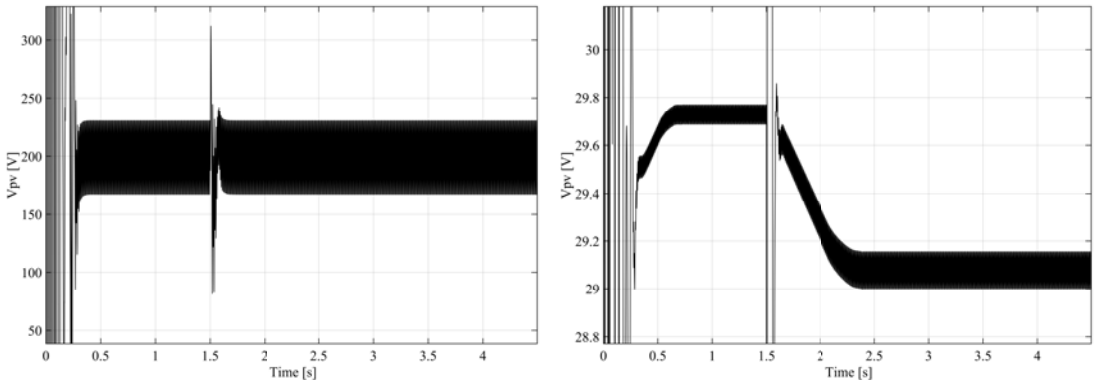

(a) DC line voltage, detail.

(b) PV panel voltage, detail.

Figure 6.13: Detail of the voltage profiles in the complete simulation.

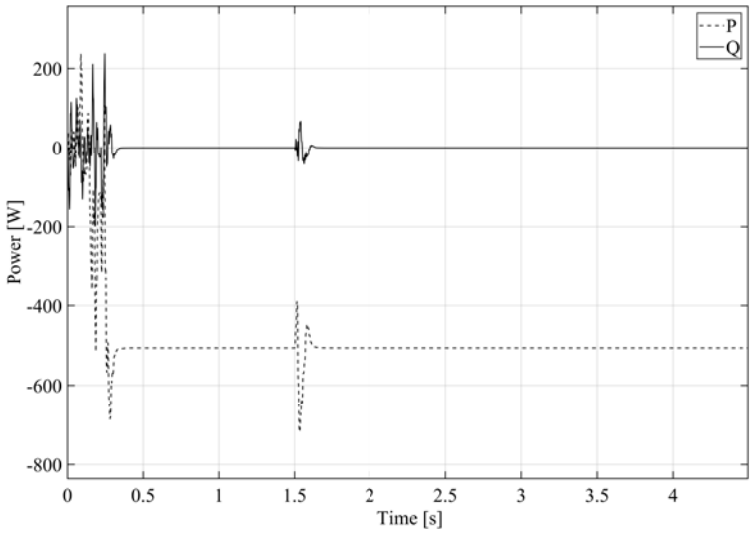

Figure 6.14: Active and reactive power curves in the complete simulation.

Chapter 7

Conclusion

This work has developed an efficient model of the buck-boost converter, that is used to control the input voltage of the photovoltaic panel, in order to operate it in optimal conditions, and to control the voltage in the DC line, maintaining it constant in spite of variations in power production and demand.

The model is able to tolerate the non linearities introduced by the PV panel and by the battery, but not the ones generated by the DC/AC converter.

The last simulation showed how the averaged model and its control are considerably affected by the non linearities introduced by the PLL, and how all the control systems must be controlled together and coordinated. In this work in fact every controller operates separately, but if they were coordinated the instability displayed at the beginning of the simulation could be avoided. The use of other control methods, besides the classic PI strategy, should be considered.

The DC/AC converter is thus the one creating the main problems in the stability of the system, also it induces a strong ripple in the DC side, with the same frequency as the one of the grid. This is also due to the fact that the averaged model has been use to represent the DC/AC converter too, which is a further simplification.

The photovoltaic panel, with the MPPT system and its converter, and the battery with its converter have shown a good response and their models can be a good starting point to develop and improve systems like this one.

When doing so, it must be kept in mind that the non linear behaviour of the different components must be considered to have a model that can be applied in real life situations, and not just for study and research purposes.

7.1 Future Works

This thesis might be useful as starting point for a future analysis on such a system. The model of the buck-boost converter has proved its validity, the photovoltaic panel s equivalent circuit and the method to calculate its parameters have displayed satisfying behaviours and, what s more important the interaction with the battery model was successful.

The model has proved it can be used to validate control assumptions of linearity and, with some precautions, it can be used for a physical implementation. Hence it is important to develop a more deep and complex study of the non linear behaviour of such system.

The correlation between the components of the DC line and the DC/AC converter must surely be improved in order to get rid of the initial instability, that delays the synchronisation of the converter and the achievement of steady state conditions; and in order to eliminate or reduce the ripple in the DC side that contributes to the instability of the system and the desynchronisation of the controllers.

Bibliography

[1] Masson G., Brunisholz M., and IEA-PVS Reporting Countries. *2016 Snapshot of Global Photovoltaic Markets*. Report. International Energy Agency (IEA), Becquerel Institute (BE), and RTS Corporation (JP), 2017.

[2] Terna. *Piano di Sviluppo 2012*. 2012. URL: `http://download.terna.it/terna/0000/0109/60.pdf`.

[3] Sechilariu M. and Locment F. *Urban DC Microgrid, Intelligent Control and Power Flow Optimization*. Ed. by Lisa Reading. 2016.

[4] Villalva M. G., Gazoli J. R., and Filho E. R. Comprehensive Approach to Modeling and Simulation of Photovoltaic Arrays . In: *IEEE Transactions on Power Electronics* 24 (5) (2009), pp. 1190 1208.

[5] Luque A. and Hegedus S. *Handbook of Photovoltaic Science and Engineering*. Wiley, 2003.

[6] Sze S. M. *Physics of Semiconductor Devices*. Wiley, 1981. Chap. 14, p. 264.

[7] Singh P. and Ravindra N. M. Temperature dependence of solar cell performance an analysis . In: *Solar Energy Materials and Solar Cells* 101 (2012), pp. 36 45.

[8] Hejri M. et al. An Analytical-Numerical Approach for Parameter Determination of a Five-Parameter Single-Diode Mode of Photovoltaic Cells and Modules . In: *International Journal of Sustainable Energy* 35 (2016), pp. 396 410.

[9] Kumar M. and Kumar A. An Efficient Parameters Extraction Technique of Photovoltaic Models for Performance Assessment . In: *Solar Energy* 158 (2017), pp. 192 206.

[10] Ayodele T. R., Ogunjuyigbe A. S. O., and Ekoh E. E. Evaluation of Numerical Algorithms Used in Extracting the Parameters of a Single-Diode Photovoltaic Model . In: *Sustainable Energy Technologies and Assessments* 13 (2016), pp. 51 59.

[11] O Donnell K. P. and Chen X. Temperature Dependence of Semiconductor Band Gaps . In: *Applied Physics Letters* 58.25 (1991), pp. 2924 2926.

[12] Tian H. et al. A Cell-to-Module-to-Array Detailed Model for Photovoltaic Panels . In: *Solar Energy* 86 (2012), pp. 2695 2706.

[13] Farhoodnea M. et al. Performance Evaluation and Characterization of a 3-kWp Grid-Connected Photovoltaic System Based on Tropical Field Experimental Results: New Results and Comparative Study . In: *Renewable and Sustainable Energy Reviews* 42 (2015), pp. 1047 1054.

[14] Bai J. et al. Development of a New Compound Method to Extract the Five Parameters of PV Modules . In: *Energy Conversion and Management* 79 (2014), pp. 294 303.

[15] Esram T. and Chapman P. L. Comparison of Photovoltaic Array Maximum Power Point Tracking Techniques . In: *IEEE Transaction on Energy Conversion* 22 (2007), pp. 439 449.

[16] Ezinwannea O., Zhongwena F., and Zhijun L. Energy Performance and Cost Comparison of MPPT Techniques for Photovoltaics and other Applications . In: *Energy Procedia* 107 (2017), pp. 297 303.

[17] Kobayashi K., Matsuo H., and Sekine Y. A Novel Optimum Operating Point Tracker of the Solar Cell Power Supply System . In: *35th Annual IEEE Power Electronics Specialists Conference* (2004), pp. 2147 2151.

[18] Veerachary M., Senjyu T., and Uezato K. Neural-Network-Based Maximum Power Point Tracking of Coupled-Inductor Interleaved-Boost-Converter-Supplied PV System Using Fuzzy Controller . In: *IEEE Transactions on Industrial Electronics* 50 (2003), pp. 749 758.

[19] All About Circuits. *Analysis of Four DC-DC Converters in Equilibrium*. 2015. URL: https://www.allaboutcircuits.com/technical-articles/analysis-of-four-dc-dc-converters-in-equilibrium/.

[20] Bakka S., Munteanu I., and Bratcu A. I. *Power Electronic Converters Modeling and Control*. Springer, 2014. Chap. 4, p. 71.

[21] Dinniyah F. S., Wahab W., and Alif M. Simulation of Buck-Boost Converter for Solar Panel Using PID Controller . In: *Energy Procedia* 115 (2017), pp. 102 113.

[22] Rashid M. H. *Power Electronics Handbook*. Academic Press, 2001.

[23] Barrera-Gallegos N., Dauphin-Tanguy G., and Guillaud X. Modal sensitivity of a reduced equivalent HVDC-VSC system . In: *2016 International Conference on Control, Decision and Information Technologies (CoDIT)*. Apr. 2016, pp. 588 593.

[24] Araujo Leão J. F. et al. Lead-Acid Battery Modeling and State of Charge Monitoring . In: *Applied Power Electronics Conference and Exposition (APEC)*. Ed. by Lima A. N. M. 2010. URL: https://www.researchgate.net/publication/224125611_Lead-Acid_Battery_Modeling_and_State_of_Charge_Monitoring.

[25] Elan s.r.l. *Batteria al Piombo 12V 250Ah Long Life*. 2017. URL: https://www.elan.an.it/images/schedetecniche/LONG_12V_01295.pdf.

[26] Yazdani A. and Iravani R. *Voltage-Sourced Converters in Power Systems*. 2010. Chap. 2, p. 101.

[27] Yazdani A. and Iravani R. *Voltage-Sourced Converters in Power Systems*. 2010. Chap. 2, p. 18.

[28] Yazdani A. and Iravani R. *Voltage-Sourced Converters in Power Systems*. 2010. Chap. 2, p. 34.

[29] Mohan N., Undeland T. M., and Robbins W. P. *Power Electronics: Converters, Applications and Design*. 2002. Chap. 8.

[30] Peralta J. et al., eds. *Dynamic Performance of Average-Value Models for Multi-terminal VSC-HVDC Systems*. IEEE Power and Energy Society General Meeting. IEEE, July 2012.

[31] Golestan S. et al. Performance Improvement of a Prefiltered Synchronous-Reference-Frame PLL by Using a PID-Type Loop Filter . In: *IEEE Transactions on Industrial Electronics* 61 (2014), pp. 3469 3479.

[32] Konstantin A. Phase-locked loops with active PI filter: the lock-in range computation . PhD thesis. University of jyväskylä, 2016. URL: https://jyx.jyu.fi/handle/123456789/50153.

[33] Zhao C. and Guo C., eds. *Complete-Independent Control Strategy of Active and Reactive Power for VSC Based HVDC System*. 2009 IEEE Power and Energy Society General Meeting. IEEE, July 2009.